(2024, under review) 001–023

Multiple reflections on Huygens' principle

Kees Wapenaar
Department of Geoscience and Engineering, Delft University of Technology, The Netherlands

18 December 2024

ABSTRACT

According to Huygens' principle, all points on a wave front act as secondary sources emitting spherical waves, and the superposition of these spherical waves forms a new wave front. In the mathematical formulation of Huygens' principle, the waves emitted by the secondary sources are represented by Green's functions. In many present-day applications of Huygens' principle, these Green's functions are replaced by their time-reversed versions, thus forming a basis for backpropagation, imaging, inversion, seismic interferometry, etc. However, when the input wave field is available only on a single open boundary, this approach has its limitations. In particular, it does not properly account for multiple reflections. This is remedied by a modified form of Huygens' principle, in which the Green's functions are replaced by focusing functions. The modified Huygens' principle forms a basis for imaging, inverse scattering, monitoring of induced sources, etc., thereby properly taking multiple reflections into account.

INTRODUCTION

Dutch mathematician, physicist and astronomer Christiaan Huygens (1629 – 1695) described light as a longitudinal mechanical wave, propagating through an ether medium. Even though, centuries later, Maxwell proposed light as a transverse electromagnetic wave and Einstein showed it doesn't need an ether to support its propagation, the early wave theoretical approach of Huygens appeared very effective in the analysis of the propagation and reflection of light. In his book "Traité de la Lumière" (Treatise on Light, presented to the Royal Academy of Sciences in 1678 and published in 1690), he explains that around each undulating particle of the matter through which a wave propagates, a spherical wave is formed of which this particle is the center. The total wave field is the superposition of these spherical waves, and the principal wave is formed by their common tangent (or envelope). This is in a nutshell Huygens' principle, and it applies to light as well as to other wave phenomena. For an extensive discussion of the work of Huygens and his important role in bridging ancient and modern science, see Moser & Robinson (2024).

Figure 1 is an illustration of Huygens' principle, applied to acoustic waves. A point source, indicated by the red star, emits a circular wave which propagates through a medium with a constant propagation velocity (the example is 2D, hence, instead of spherical waves we have circular waves). At a certain time this wave reaches a screen with a small opening (Figure 1a). The wave field in this opening acts as a secondary source, which emits a circular wave into the half-space above the screen. Figure 1b shows a similar setup, but this time the screen has many small openings, which all act as secondary sources (indicated by the blue stars), emitting circular waves at the time the original wave reaches these openings. Hence, the field above the screen consists of a superposition of circular waves. The envelope of these superposed waves approximately forms a circular wave, resembling the wave that would be radiated by the original point source in absence of the screen. In Figure 1c the screen contains one large opening. All points in this opening act as secondary sources (indicated by the dense distribution of blue stars) and the superposition of the circular waves above the screen has indeed converged to the circular wave radiated by the original source.

Huygens' principle has found many applications in optics, acoustics and other fields in which wave propagation and scattering plays a role. In this paper we restrict ourselves to applications in acoustics and geophysics, in particular for wave field extrapolation. Traditionally, the waves emitted by the secondary sources in Huygens' prin-

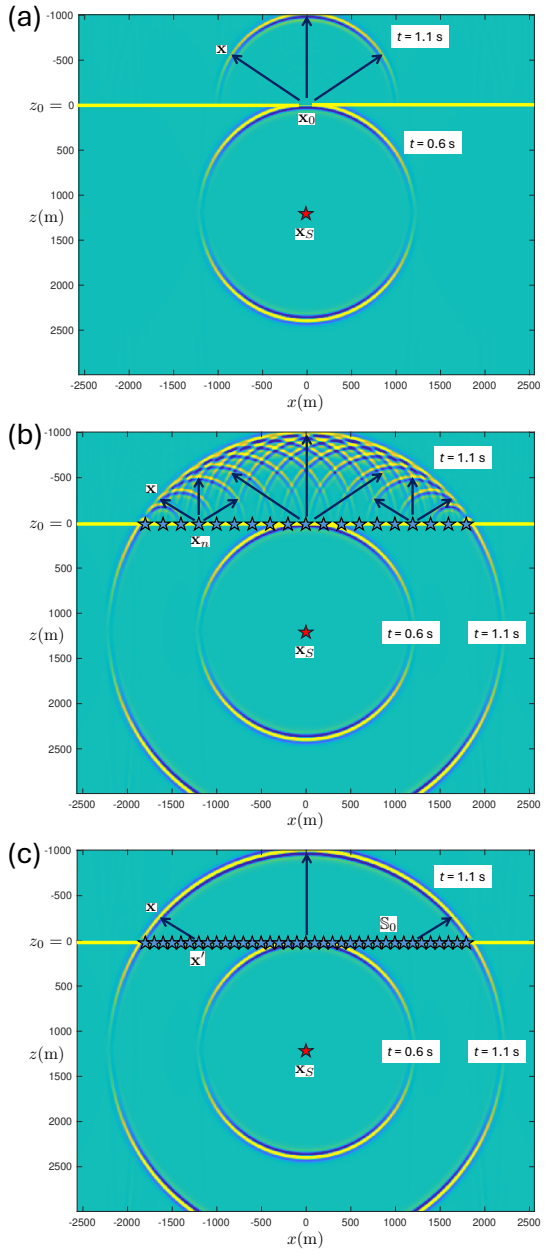

Figure 1. *Illustration of Huygens' principle for acoustic waves in a homogeneous medium (see text for explanations). Animations are available at https://www.keeswapenaar.nl/HP2/Movie1a.mp4, https://www.keeswapenaar.nl/HP2/Movie1b.mp4 and https://www.keeswapenaar.nl/HP2/Movie1c.mp4. (Links to animations will be modified in the final version of this paper).*

ciple are represented by Green's functions. We start by reviewing applications of the traditional Huygens' principle in forward and inverse wave field extrapolation. It appears that with the traditional Huygens' principle, internal multiples are not correctly handled in inverse extrapolation through an inhomogeneous medium. Next, we discuss a modified version of Huygens' principle, in which the Green's functions are replaced by focusing functions. We indicate applications of this modified Huygens' principle and show that the aforementioned limitations are circumvented.

The style of the main text is informal, with an emphasis on explanations of the different forms of Huygens' principle, using simple mathematics. More detailed derivations can be found in the appendices.

TRADITIONAL HUYGENS' PRINCIPLE, USING GREEN'S FUNCTIONS

Forward wave field extrapolation through a homogeneous medium

We discuss some mathematics behind Huygens' principle, as illustrated in Figure 1, and use this as a starting point for the discussion of forward wave field extrapolation. We define a Cartesian coordinate system, with the z-axis pointing downward and coordinate vector $\mathbf{x}$ denoting position in this system. For the 3D situation this vector is defined as $\mathbf{x} = (x, y, z)$. Whereas most of the theory in this paper holds for 3D, the examples are 2D, in which case the coordinate vector is defined as $\mathbf{x} = (x, z)$. Time is denoted by t.

Let $\mathbf{x}_S$ denote the position of a monopole source (in Figure 1 it is defined as $\mathbf{x}_S = (0, 1200)$ m). We define the acoustic Green's function $G(\mathbf{x}, \mathbf{x}_S, t)$ (named after George Green, 1793 – 1841) as the response to an impulsive monopole source at $\mathbf{x}_S$ and $t = 0$, observed at $\mathbf{x}$ as a function of t. The Green's function is a causal function of time, meaning $G(\mathbf{x}, \mathbf{x}_S, t) = 0$ for $t < 0$. The source of the Green's function is a volume-injection rate source, see Appendix A–1 for further details. When the source in an actual situation is not an impulse but a transient wavelet $s(t)$, then the observed acoustic pressure is given by the convolution of the Green's function with the wavelet, according to

$$p(\mathbf{x}, t) = \int_0^\infty G(\mathbf{x}, \mathbf{x}_S, t')s(t - t')\mathrm{d}t'. \qquad (1)$$

To simplify the notation, here and in subsequent sections,

we introduce the convolutional symbol $*$ and replace the integral notation of equation (1) by

$$p(\mathbf{x},t) = G(\mathbf{x},\mathbf{x}_S,t) * s(t). \tag{2}$$

The wave fronts in Figure 1 below the screen are described by this equation. The source function $s(t)$ is a Ricker wavelet with a central frequency of 20 Hz and $G(\mathbf{x},\mathbf{x}_S,t)$ is the 2D Green's function in a homogeneous lossless medium with propagation velocity $c = 2000$ m/s and mass density $\rho = 1000$ kg/m^3 (hence, the wavelength at the central frequency is 100 m). The amplitudes along the wave fronts are tapered at large propagation angles (relative to the vertical axis) and waves reflected by the screen are not shown. Let $\mathbf{x}_0 = (x_0, z_0)$ denote the position of the opening in the screen in Figure 1a, with z_0 being the depth level of the screen (with $z_0 = 0$ m here and in subsequent figures). According to Huygens' principle, the acoustic pressure at this position, $p(\mathbf{x}_0,t)$, acts as a secondary source for the wave field above the screen, hence, analogous to equation (2), this is given by

$$p(\mathbf{x},t) \propto G(\mathbf{x},\mathbf{x}_0,t) * p(\mathbf{x}_0,t), \tag{3}$$

where the symbol $\propto$ means "proportional to". Next, let $\mathbf{x}_n = (n\Delta x, z_0)$, $n = -N, \ldots, -1, 0, 1, \ldots, N$, denote the positions of the openings in the screen in Figure 1b (with $N = 9$ and $\Delta x = 200$ m). Then, according to Huygens' superposition principle, the wave field in the half-space above the screen can be expressed as

$$p(\mathbf{x},t) \propto \sum_{n=-N}^{N} G(\mathbf{x},\mathbf{x}_n,t) * p(\mathbf{x}_n,t). \tag{4}$$

Next, for the situation of one large opening in the screen, as in Figure 1c, we reduce the distance between the secondary sources to $\Delta x = 10$ m. Since this is significantly smaller than the central wavelength of 100 m, we now have effectively a continuum of secondary sources and we replace the summation by an integration, according to

$$p(\mathbf{x},t) \propto \int_{\mathbb{S}_0} G(\mathbf{x},\mathbf{x}',t) * p(\mathbf{x}',t)\mathrm{d}\mathbf{x}', \tag{5}$$

where $\mathbb{S}_0$ denotes the integration boundary (the opening in the screen as in Figure 1c, or an infinite horizontal boundary in absence of the screen). For the 2D situation considered here, this is a 1D integral over x'; for the 3D situation it is a 2D integral over x' and y'. In both cases z' is fixed and equal to z_0, being the depth of integration boundary $\mathbb{S}_0$.

Up to this point, we captured the physical arguments of Huygens in mathematical form (the mathematics presented here was not yet available in the time of Huygens). Using only physical arguments, the proportionality factor remains unknown. In the 19th century, Kirchhoff, Helmholtz, Rayleigh and others derived expressions which formalize Huygens' principle. In Appendix B we summarize their derivation and obtain the following more precise form of equation (5)

$$p(\mathbf{x},t) = -2\int_{\mathbb{S}_0} G_\mathrm{d}(\mathbf{x},\mathbf{x}',t) * p(\mathbf{x}',t)\mathrm{d}\mathbf{x}', \tag{6}$$

for $\mathbf{x}$ above $\mathbb{S}_0$. Here $G_\mathrm{d}(\mathbf{x},\mathbf{x}',t)$ is the response to an impulsive dipole source at $\mathbf{x}'$ and $t = 0$, with $\mathbf{x}'$ on $\mathbb{S}_0$, see Figure 2 (actually we already used this dipole Green's function in generating the example in Figure 1). This dipole Green's function is further specified in Appendix A–3. The minus-sign in equation (6) stems from the definition of the dipole (it is oriented with respect to the positive z-axis, whereas in equation (6) it radiates in the negative z-direction). The factor 2 in equation (6) is explained later.

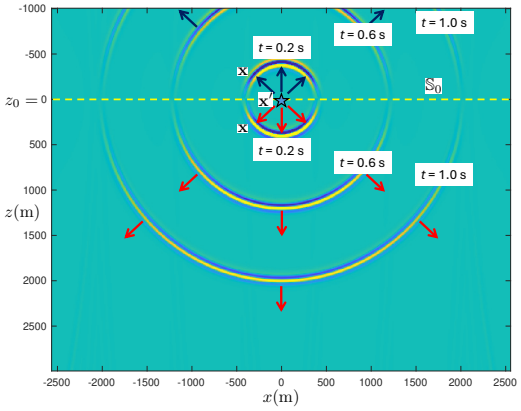

Figure 2. *Dipole Green's function $G_\mathrm{d}(\mathbf{x},\mathbf{x}',t)$ (convolved with a Ricker wavelet to get a nicer display) in a homogeneous medium, for a dipole at $\mathbf{x}'$ on $\mathbb{S}_0$ at depth z_0. Animation at https://www.keeswapenaar.nl/HP2/Movie2.mp4.*

Huygens' wave-theoretical description of light was not immediately accepted. One of the reasons was that it does not explain why the secondary sources radiate only forward, i.e., in the direction of the principal wave. If each point in a wave field acts as a secondary source, one would expect it to radiate in all directions (like the dipole source of the Green's function in Figure 2). Consequently, the envelope of the superposed waves of all secondary sources on a plane would consist of two contributions: one propagating forward, in the direction of the original wave, and one propagating backward, against the direction of the original wave. In the time of Huygens it was not clear why the secondary sources do not give rise to this backward

propagating wave. This was seen as a serious drawback of Huygens' wave-theoretical approach. Newton's competing theory (light consisting of particles moving along straight lines) did not have this drawback, but it had other shortcomings, such as not explaining diffraction and interference. All in all, Huygens' wave theory has withstood the test of time.

To understand why the secondary sources generate only the forward propagating wave, consider the Kirchhoff-Helmholtz integral in equation (B-8). This integral contains monopole and dipole Green's functions, driven by the particle velocity and acoustic pressure, respectively, at the horizontal boundary $\mathbb{S}_0$. Equation (B-8) states that the combination of secondary monopole and dipole responses yields the forward propagating wave in the half-space above $\mathbb{S}_0$, whereas their contributions cancel in the half-space below $\mathbb{S}_0$. Moreover, for the homogeneous medium configuration of Figure 1, the secondary monopoles and dipoles give equal contributions to the wave field above $\mathbb{S}_0$, so one of the terms can be omitted and the other term doubled, yielding equation (6) and explaining the factor 2 in this equation. Whereas equation (B-8) holds for $\mathbf{x}$ at either side of $\mathbb{S}_0$, equation (6) only applies for $\mathbf{x}$ above $\mathbb{S}_0$.

Huygens' principle was developed in the pre-industrial age. At the time it was merely meant to explain the physics of wave propagation. Technological developments in the 20th century enabled many other interesting applications of Huygens' principle. For example, in equation (6), the wave field $p(\mathbf{x}', t)$ at $\mathbb{S}_0$ can be replaced by electric signals that are fed to a dense array of piezoelectric transducers which emit ultrasound. Equation (6) then describes the synthesized wave field emitted by the array into the half-space above $\mathbb{S}_0$. On the other hand, digitized measurements of an acoustic or seismic wave field $p(\mathbf{x}', t)$ at $\mathbb{S}_0$ can be fed to a computer and equation (6) can be evaluated numerically to compute the wave field $p(\mathbf{x}, t)$ at any position $\mathbf{x}$ in the half-space above $\mathbb{S}_0$. The latter application is wave field extrapolation (Berkhout 1985). In practice, the convolution along the time coordinate is often replaced by a multiplication in the frequency domain, see equation (B-9), but for clarity we keep our expressions in the time domain because this appeals better to the physics of Huygens' principle.

In equation (6), $\mathbf{x}$ is assumed to be situated in the half-space above $\mathbb{S}_0$, whereas the source (or source distribution) of the wave field $p(\mathbf{x}', t)$ resides in the half-space below $\mathbb{S}_0$. For this situation we speak of *forward* wave field extrapolation, since the direction of extrapolation (upward from $\mathbb{S}_0$ to $\mathbf{x}$ above $\mathbb{S}_0$) corresponds to the direction of the upgoing wave field $p(\mathbf{x}', t)$ at $\mathbb{S}_0$. Since this is the direction of the negative z-axis, we indicate this with a superscript $-$ as follows

$$p^-(\mathbf{x}, t) = -2 \int_{\mathbb{S}_0} G_\mathrm{d}(\mathbf{x}, \mathbf{x}', t) * p^-(\mathbf{x}', t) \mathrm{d}\mathbf{x}', \qquad (7)$$

for $\mathbf{x}$ above $\mathbb{S}_0$. Similarly, for forward extrapolation of a downgoing field, indicated with a superscript $+$, we can derive in a similar way

$$p^+(\mathbf{x}, t) = 2 \int_{\mathbb{S}_0} G_\mathrm{d}(\mathbf{x}, \mathbf{x}', t) * p^+(\mathbf{x}', t) \mathrm{d}\mathbf{x}', \qquad (8)$$

for $\mathbf{x}$ below $\mathbb{S}_0$ (here the source is assumed to be situated in the half-space above $\mathbb{S}_0$). Note that the dipole Green's function $G_\mathrm{d}(\mathbf{x}, \mathbf{x}', t)$ for $\mathbf{x}$ below $\mathbb{S}_0$ has a sign opposite to that for $\mathbf{x}$ above $\mathbb{S}_0$, see Figure 2. This compensates for the different signs in front of the integrals in equations (7) and (8).

Inverse wave field extrapolation through a homogeneous medium

We start this section with discussing an intuitive modification of Huygens' principle for backpropagation. We consider again the acoustic pressure $p(\mathbf{x}, t)$ in a homogeneous lossless medium, in response to a source in the lower half-space (at $\mathbf{x}_S = (0, 1200)$ m), observed at $\mathbf{x}_n = (n\Delta x, z_0)$ at $\mathbb{S}_0$, with $n = -N, \ldots, -1, 0, 1, \ldots, N$ (with $N = 50$ and $\Delta x = 200$ m). In equation (4) we replace the Green's function by the time-reversed Green's function $G_\mathrm{d}(\mathbf{x}, \mathbf{x}_n, -t)$ (i.e., the time-reversal of the dipole Green's function shown in Figure 2). Hence, we evaluate the expression

$$\langle p(\mathbf{x}, t) \rangle \propto 2 \sum_{n=-N}^{N} G_\mathrm{d}(\mathbf{x}, \mathbf{x}_n, -t) * p(\mathbf{x}_n, t), \qquad (9)$$

for $\mathbf{x}$ in the half-space below $\mathbb{S}_0$. The notation $\langle p(\mathbf{x}, t) \rangle$ means "estimate of $p(\mathbf{x}, t)$." Whereas in equation (4) the Green's function $G(\mathbf{x}, \mathbf{x}_n, t)$ forward propagates the field of the secondary sources $p(\mathbf{x}_n, t)$ into the half-space above $\mathbb{S}_0$, in equation (9) the time-reversed Green's function $G_\mathrm{d}(\mathbf{x}, \mathbf{x}_n, -t)$ backpropagates the field of the secondary sources $p(\mathbf{x}_n, t)$ into the half-space below $\mathbb{S}_0$ (Schneider 1978). The result $\langle p(\mathbf{x}, t) \rangle$ for $t = 0.4$ s is shown in Figure 3a. This figure illustrates Huygens' superposition principle for backpropagation. The envelope of the superposed circular waves approximately forms a circular wave, resembling the wave emitted by the original point source at $\mathbf{x}_S$, observed above this point source at $t = 0.4$ s. Figure 3b shows $\langle p(\mathbf{x}, t) \rangle$ for $t = 0$ s. Here a focus is formed at the position of the original point source. Since there is no sink at $\mathbf{x}_S$ to absorb the focused field, $\langle p(\mathbf{x}, t) \rangle$ does not

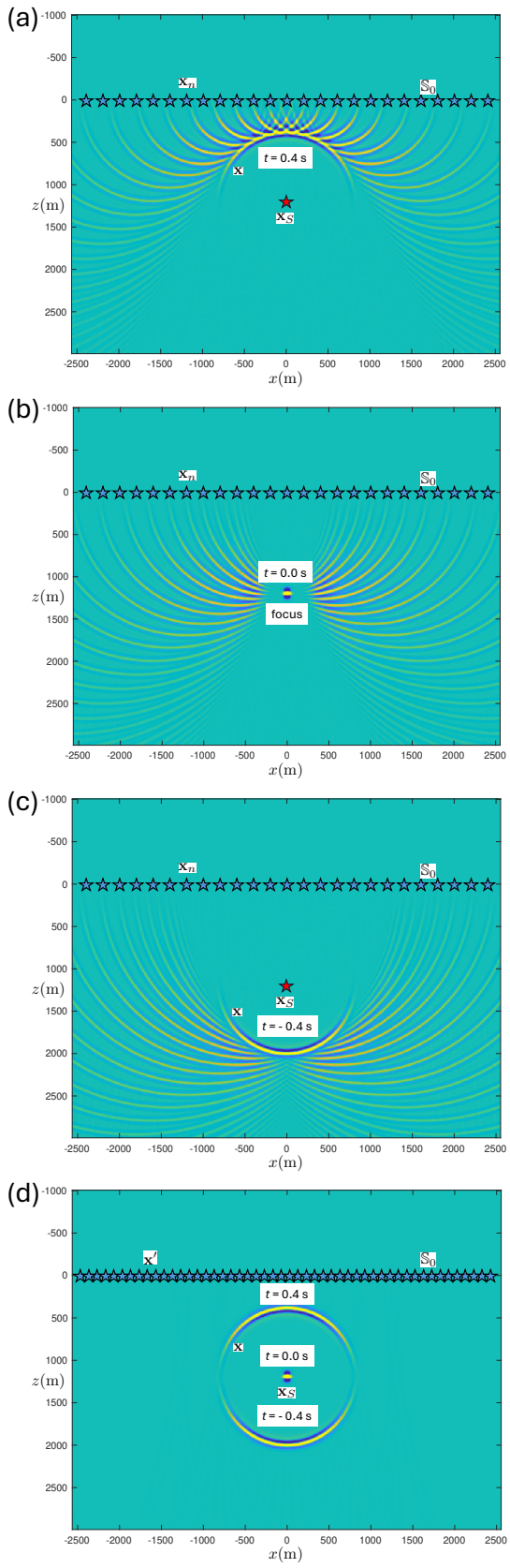

Figure 3. *(a)–(c) Illustration of Huygens' principle for backpropagation of acoustic waves in a homogeneous medium, according to equation (9). (d) Idem, according to equation (10). Animations at https://www.keeswapenaar.nl/HP2/Movie3a.mp4 and https://www.keeswapenaar.nl/HP2/Movie3b.mp4.*

vanish when we continue the backpropagation to negative times, as is shown in Figure 3c for $t = -0.4$ s. Next, we replace the summation in equation (9) by an integration, according to

$$\langle p(\mathbf{x},t)\rangle = 2\int_{\mathbb{S}_0} G_{\mathrm{d}}(\mathbf{x},\mathbf{x}',-t) * p(\mathbf{x}',t)\mathrm{d}\mathbf{x}' \qquad (10)$$

(but in the numerical implementation we actually evaluate equation (9), with Δx reduced to $\Delta x = 10$ m and $N = 1000$). Figure 3d shows a superposition of snapshots of $\langle p(\mathbf{x},t)\rangle$ for $t = 0.4$ s, $t = 0$ s and $t = -0.4$ s. In the left-hand side of equation (10) we still use the notation $\langle p(\mathbf{x},t)\rangle$, indicating an approximation of $p(\mathbf{x},t)$. The actual response to a point source at $\mathbf{x}_S$ is causal and consists of circular wave fronts around $\mathbf{x}_S$ at positive times only, whereas Figure 3d shows an incomplete response at positive time (a half-circle above $\mathbf{x}_S$), and a non-existing response at negative time (a half-circle below $\mathbf{x}_S$). In Appendix C we review a step-by-step derivation of equation (10). It starts with an exact expression, containing time-reversed monopole and dipole Green's functions (equation (C-2)). Under specific circumstances, which includes ignoring evanescent waves, this leads to equation (C-4), which has three terms on the right-hand side. The second of these terms is the integral in the right-hand side of equation (10). For the homogeneous medium configuration in Figure 3, evaluating the first term of equation (C-4) would suppress the acausal response at negative time and evaluating the third term would restore the missing half-circle below $\mathbf{x}_S$ at positive time. Since these terms require knowledge of the source at $\mathbf{x}_S$ and measurements of its response at a boundary below the source, they cannot be evaluated in most practical situations. By ignoring the first and third term in equation (C-4), we are left with equation (10), with the limitations discussed above. For an inhomogeneous medium the limitations are even more severe, as we will see in the next section.

Unlike equation (6), which formalizes Huygens' explanation of the physics of wave propagation, equation (10) with the time-reversed Green's function does not describe a physical situation. However, it can be used for numerical wave field extrapolation of an upgoing wave field $p(\mathbf{x}',t)$, measured at $\mathbb{S}_0$, to any position below $\mathbb{S}_0$ and above the source. Here we speak of *inverse* wave field extrapolation, since the direction of extrapolation (downward from $\mathbb{S}_0$ to $\mathbf{x}$ below $\mathbb{S}_0$) is opposite to the direction of the upgoing wave field $p(\mathbf{x}',t)$ at $\mathbb{S}_0$. We indicate upgoing wave fields again with a superscript $-$ and replace equation (10) by

$$p^{-}(\mathbf{x},t) = 2\int_{\mathbb{S}_0} G_{\mathrm{d}}(\mathbf{x},\mathbf{x}',-t) * p^{-}(\mathbf{x}',t)\mathrm{d}\mathbf{x}', \qquad (11)$$

for $\mathbf{x}$ below $\mathbb{S}_0$. As long as $\mathbf{x}$ is above the source in the lower half-space, equation (11) describes the complete upgoing wave field at $\mathbf{x}$, see Figure 3 (in this case the only approximation is the neglection of evanescent waves). When the lower half-space is source-free, equation (11) even holds for the entire lower half-space. Similarly, for inverse extrapolation of a downgoing wave field we can derive in a similar way

$$p^+(\mathbf{x},t) = -2\int_{\mathbb{S}_0} G_{\rm d}(\mathbf{x},\mathbf{x}',-t) * p^+(\mathbf{x}',t){\rm d}\mathbf{x}', \qquad (12)$$

for $\mathbf{x}$ above $\mathbb{S}_0$. As long as $\mathbf{x}$ is below the source in the upper half-space, equation (12) describes the complete downgoing wave field at $\mathbf{x}$. When the upper half-space is source-free, equation (12) holds for the entire upper half-space.

Equations (11) and (12) are the basic expressions for inverse wave field extrapolation through a homogeneous lossless medium, as applied in acoustic and seismic imaging. They can be implemented in the space-time domain, as in Kirchhoff migration (Schneider 1978; Tygel *et al.* 2000) and reverse-time migration (Whitmore 1983; McMechan 1983), in the space-frequency domain, as in seismic inversion (Cohen *et al.* 1986) and seismic migration (Berkhout 1985), or in the wavenumber-frequency domain, as in migration with the phase-shift method (Gazdag 1978).

Another application of equation (10) is obtained when we revert the time coordinate, according to

$$2\int_{\mathbb{S}_0} G_{\rm d}(\mathbf{x},\mathbf{x}',t) * p(\mathbf{x}',-t){\rm d}\mathbf{x}'. \qquad (13)$$

Note that $G_{\rm d}(\mathbf{x},\mathbf{x}',t)$ is again the causal response to a dipole at $\mathbf{x}'$ on $\mathbb{S}_0$. Expression (13) underlies the principle of time-reversed acoustics, as advocated by Fink (1992) and coworkers. In this situation, $p(\mathbf{x}',-t)$ represents the time-reversal of measurements at $\mathbb{S}_0$, which are fed to a dense array of piezoelectric transducers which emit ultrasound. Equation (13) thus describes the synthesized wave field emitted by the array into the half-space below $\mathbb{S}_0$. If we interchange the labels for positive and negative times in Figure 3, this figure shows the wave field at $t = -0.4$ s converging to the position of the original source, the focused field at $t = 0$ s, and the field at $t = 0.4$ s diverging from the focus. Note that in this case the focused field acts as a downward radiating virtual source. A further discussion of time-reversed acoustics is beyond the scope of this paper.

Inverse wave field extrapolation through an inhomogeneous medium

We discuss Huygens' principle for backpropagation through an inhomogeneous lossless medium. To show the essence, we consider for simplicity the horizontally layered medium of Figure 4, with interfaces (indicated by the yellow solid lines) at $z = 500$ m and $z = 1500$ m. The propagation velocity c is taken constant throughout at 2000 m/s. The mass density ρ in the half-spaces $z < 500$ m and $z > 1500$ m equals 1000 kg/m^3 and in the layer $500 < z < 1500$ m it equals 4000 kg/m^3. We place again a monopole source at $\mathbf{x}_S = (0, 1200)$ m (indicated by the red star), between the two interfaces. The source function is again a Ricker wavelet $s(t)$ with a central frequency of 20 Hz. The response to this source, $p(\mathbf{x},t) = G(\mathbf{x},\mathbf{x}_S,t) * s(t)$, is shown in Figures 4a – 4d for $t = 0.2$ s, $t = 0.4$ s, $t = 0.6$ s and $t = 0.8$ s (note that the amplitudes along the wave fronts are again tapered at large propagation angles). The interfaces at $z = 500$ m and $z = 1500$ m partially reflect and partially transmit the waves. Figure 4d shows the first multiply reflected wave.

For the same layered medium, the dipole Green's function $G_{\rm d}(\mathbf{x},\mathbf{x}',t)$, for a dipole at $\mathbf{x}'$ on $\mathbb{S}_0$, is shown in Figure 5. Snapshots of this Green's function for $t = 0.2$ s and $t = 0.4$ s are shown in Figure 5a, whereas Figure 5b shows a snapshot for $t = 1.4$ s. Figure 5c is a cross-section of $G_{\rm d}(\mathbf{x},\mathbf{x}',t)$ along a vertical line through the dipole source, as a function of depth z and time t. The vertical dashed lines in this figure at $t = 0.2$ s, $t = 0.4$ s and $t = 1.4$ s correspond to the vertical dashed lines in the snapshots in Figures 5a and 5b. The vertical solid line in Figure 5c at $t = 0$ s indicates the causality condition, which states that $G_{\rm d}(\mathbf{x},\mathbf{x}',t)$ is non-zero only after the source at $t = 0$ (hence, right of this line). Figure 5d is a ray diagram of this dipole Green's function.

We use the time-reversal of the dipole Green's function of Figure 5 to backpropagate the acoustic pressure wave field of Figure 4 from $\mathbb{S}_0$ to any point $\mathbf{x}$ below $\mathbb{S}_0$. First we use the discretized form of Huygens' principle, as formulated by equation (9), with $\mathbf{x}_n = (n\Delta x, z_0)$, $\Delta x = 200$ m and $N = 50$. The results $\langle p(\mathbf{x},t)\rangle$ for $t = 0.8$ s and $t = 0.4$ s are shown in Figures 6a and 6b. Compare these figures with Figures 4d and 4b, which show the desired field $p(\mathbf{x},t)$ at the same time instants. It appears that the envelopes of the superposed waves in Figures 6a and 6b resemble parts of the desired field, but significant parts are missing (in particular the downgoing field in the lower half-space), the amplitudes of the reflected waves are too low, and circular ghost events appear in

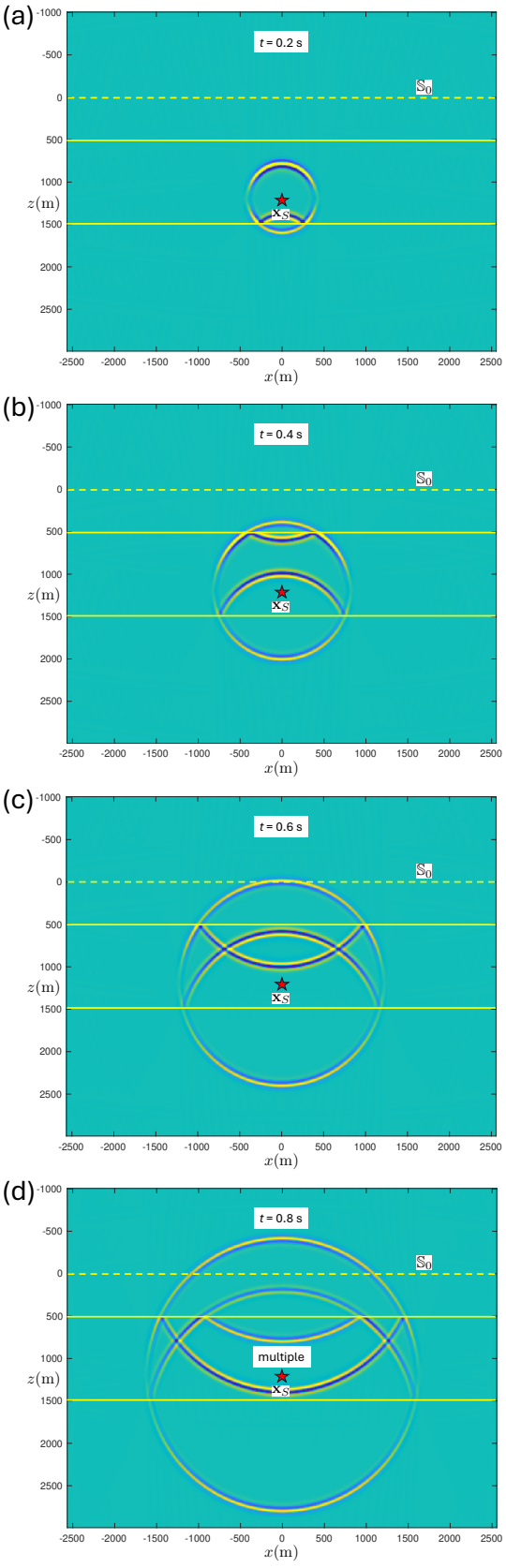

Figure 4. *Wave field* $p(\mathbf{x},t) = G(\mathbf{x},\mathbf{x}_S,t) * s(t)$ *in a layered medium, for a monopole at* $\mathbf{x}_S$*. Animation at https://www.keeswapenaar.nl/HP2/Movie4.mp4.*

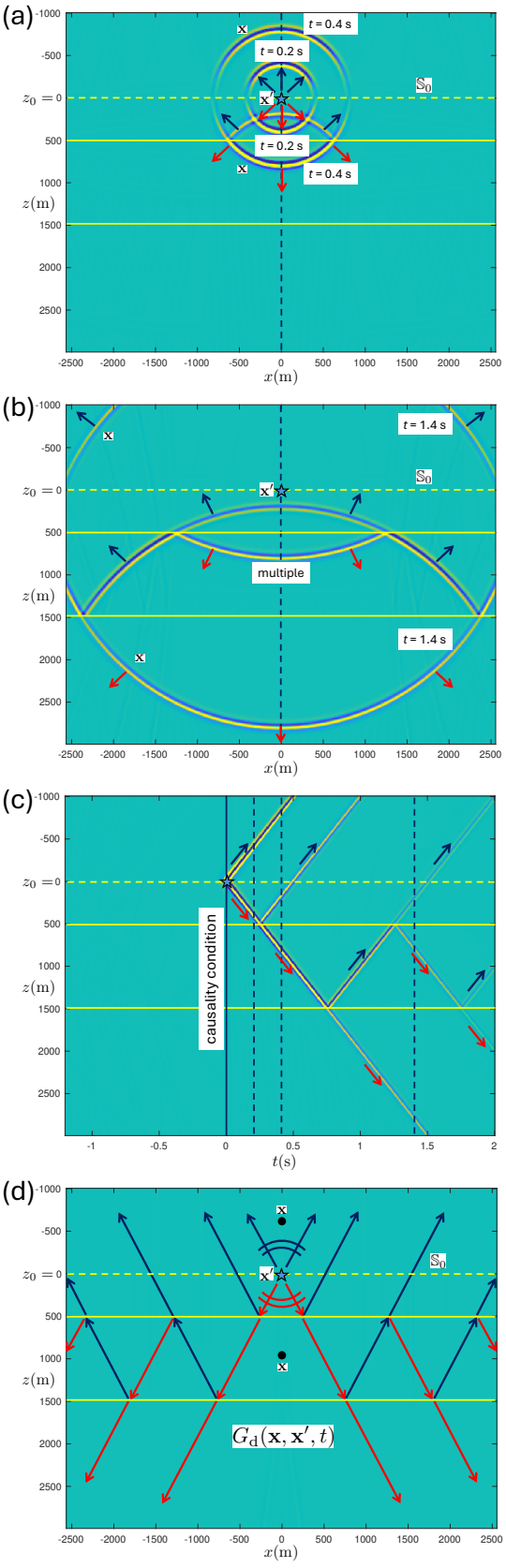

Figure 5. *(a),(b) Dipole Green's function* $G_{\mathrm{d}}(\mathbf{x},\mathbf{x}',t)$ *(convolved with a Ricker wavelet) in a layered medium, for a dipole at* $\mathbf{x}'$ *on* $\mathbb{S}_0$ *at depth* z_0*. (c) Cross-section at* $x = x' = 0$*. (d) Ray diagram. Animation at https://www.keeswapenaar.nl/HP2/Movie5.mp4.*

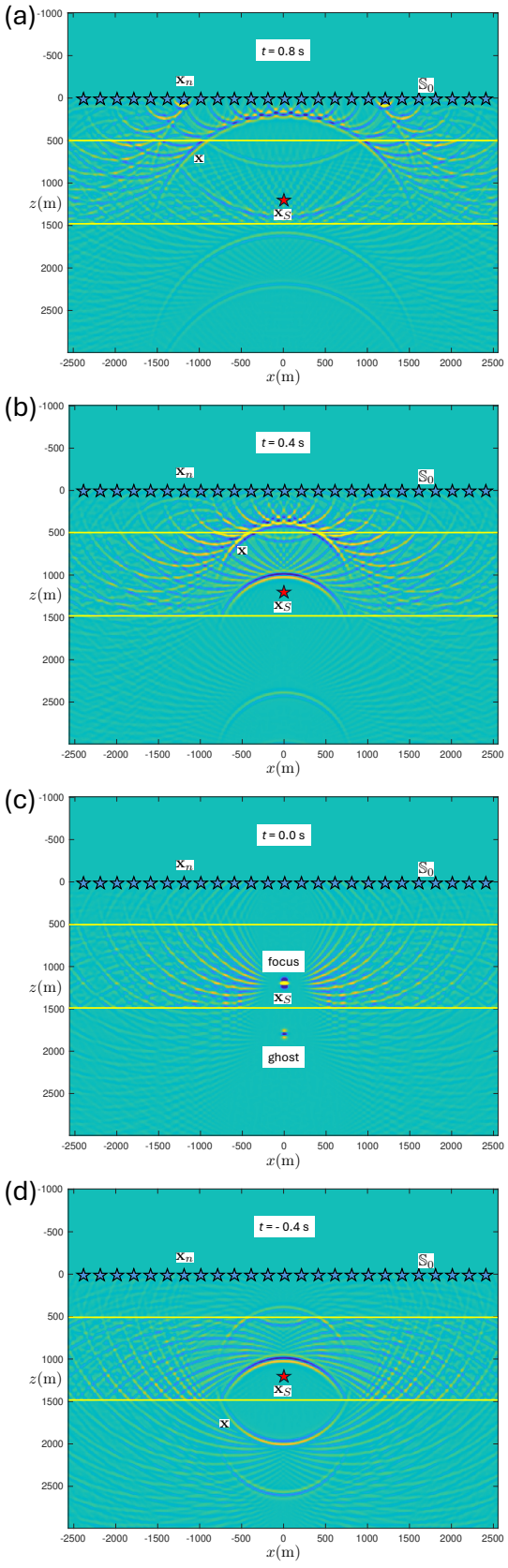

Figure 6. *Illustration of Huygens' principle for backpropagation of acoustic waves in a layered medium (equation (9), with the dipole Green's function of Figure 5). Animations at https://www.keeswapenaar.nl/HP2/Movie6a.mp4 and https://www.keeswapenaar.nl/HP2/Movie6b.mp4.*

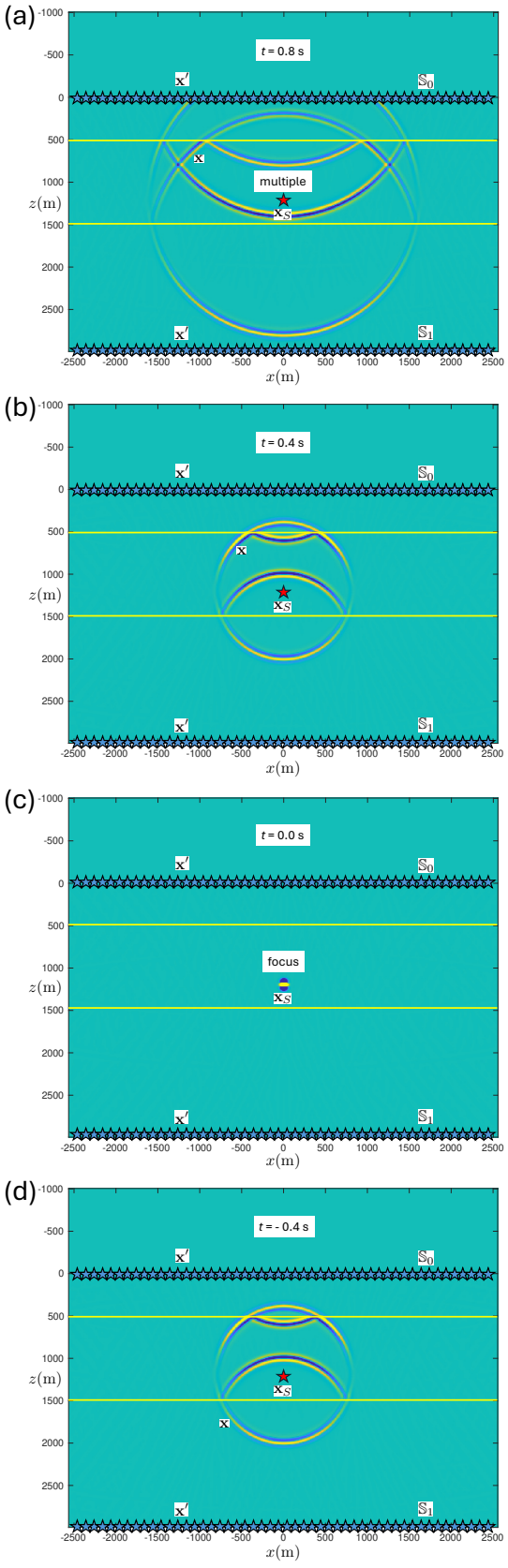

Figure 7. *Illustration of Huygens' principle for backpropagation of acoustic waves in a layered medium from two enclosing boundaries (equation (14)). Animations at https://www.keeswapenaar.nl/HP2/Movie7a.mp4 and https://www.keeswapenaar.nl/HP2/Movie7b.mp4.*

the lower half-space. Figure 6c shows $\langle p(\mathbf{x},t)\rangle$ for $t = 0$ s. Apart from the focus at the position of the original point source, a ghost focus is formed below the second interface. Figure 6d shows $\langle p(\mathbf{x},t)\rangle$ for $t = -0.4$ s. Clearly $\langle p(\mathbf{x},t)\rangle$ does not vanish for negative times. The situation is more complex than in Figure 3, which is the result of applying equation (9) in a homogeneous medium. In particular, reflected waves are not correctly backpropagated by the time-reversed dipole Green's function of the layered medium.

Next, we use the integral form of Huygens' principle, as formulated by equation (10), which we extend with a second integral over a boundary $\mathbb{S}_1$ (at $z_1 = 3000$ m) below the source, hence

$$\begin{aligned}\langle p(\mathbf{x},t)\rangle &= 2\int_{\mathbb{S}_0} G_{\mathrm{d}}(\mathbf{x},\mathbf{x}',-t) * p(\mathbf{x}',t)\mathrm{d}\mathbf{x}' \\ &- 2\int_{\mathbb{S}_1} G_{\mathrm{d}}(\mathbf{x},\mathbf{x}',-t) * p(\mathbf{x}',t)\mathrm{d}\mathbf{x}', \qquad (14)\end{aligned}$$

for $\mathbf{x}$ between $\mathbb{S}_0$ and $\mathbb{S}_1$. The results $\langle p(\mathbf{x},t)\rangle$ for $t = 0.8$ s and $t = 0.4$ s are shown in Figures 7a and 7b. These results accurately resemble the desired field $p(\mathbf{x},t)$, shown in Figures 4d and 4b, respectively, including the internal multiple reflections. Figure 7c, which shows $\langle p(\mathbf{x},t)\rangle$ for $t = 0$ s, contains a single focus at the position of the original point source. Finally, Figure 7d shows $\langle p(\mathbf{x},t)\rangle$ for $t = -0.4$ s, which again appears to be non-zero. Comparing equation (14) with equation (C-4), we find that $\langle p(\mathbf{x},t)\rangle$ consists of two contributions, according to

$$\langle p(\mathbf{x},t)\rangle = p(\mathbf{x},t) + G(\mathbf{x},\mathbf{x}_S,-t) * s(t). \qquad (15)$$

The second term in this expression explains the contribution at negative time in Figure 7d.

In most practical situations, measurements are available only at a single boundary, say $\mathbb{S}_0$, meaning that the second integral in equation (14) cannot be evaluated. Hence, we are left with the integral along $\mathbb{S}_0$, as formulated by equation (10), but with $G_{\mathrm{d}}(\mathbf{x},\mathbf{x}',-t)$ defined in the inhomogeneous medium. Similar as for a homogeneous medium, we can reformulate this again into equation (11), which then describes approximate inverse extrapolation of upgoing waves $p^-(\mathbf{x},t)$ from $\mathbb{S}_0$ through an inhomogeneous medium, to $\mathbf{x}$ below $\mathbb{S}_0$ and above the source in the lower half-space. As we have seen above, this approximation does not properly handle multiple reflections, so it only accounts for primary waves. Moreover, even for these primary waves, amplitude errors occur, which are proportional to multiple reflections (see Wapenaar *et al.* (1989) for a detailed analysis). Despite these approximations, equation (11), with the dipole Green's function defined in the inhomogeneous medium, forms the basis for many acoustic and seismic imaging schemes, including reverse time migration, time-reversed acoustics, etc. The approximations are acceptable as long as the contrasts in the medium are sufficiently small so that internal multiples can be ignored. For situations in which internal multiples cannot be ignored, other approaches are needed. One of these approaches is the replacement of the dipole Green's functions by focusing functions. This modification of Huygens' principle is the subject of the next section.

We conclude this section by deriving a representation for the homogeneous Green's function from equations (14) and (15). Using equation (2) for the first term in equation (15), we observe that this equation can be written as $\langle p(\mathbf{x},t)\rangle = G_{\mathrm{h}}(\mathbf{x},\mathbf{x}_S,t) * s(t)$, where $G_{\mathrm{h}}(\mathbf{x},\mathbf{x}_S,t)$ is the homogeneous Green's function, defined as

$$G_{\mathrm{h}}(\mathbf{x},\mathbf{x}_S,t) = G(\mathbf{x},\mathbf{x}_S,t) + G(\mathbf{x},\mathbf{x}_S,-t), \qquad (16)$$

see Appendix A-2 (here "homogeneous" refers to the fact that the wave equation for G_{h} has no source term, hence, it is a homogeneous differential equation). Next, using this in the left-hand side of equation (14) and using equation (2) for $p(\mathbf{x}',t)$ in the right-hand side of equation (14), we obtain (after deleting the convolution with $s(t)$ on both sides) the following representation for the homogeneous Green's function in an inhomogeneous lossless medium

$$\begin{aligned}G_{\mathrm{h}}(\mathbf{x},\mathbf{x}_S,t) &= 2\int_{\mathbb{S}_0} G_{\mathrm{d}}(\mathbf{x},\mathbf{x}',-t) * G(\mathbf{x}',\mathbf{x}_S,t)\mathrm{d}\mathbf{x}' \\ &- 2\int_{\mathbb{S}_1} G_{\mathrm{d}}(\mathbf{x},\mathbf{x}',-t) * G(\mathbf{x}',\mathbf{x}_S,t)\mathrm{d}\mathbf{x}' \qquad (17)\end{aligned}$$

(Porter 1970; Oristaglio 1989). This representation forms the basis for holographic imaging and inverse scattering methods. If we use the source-receiver reciprocity relation $G(\mathbf{x}',\mathbf{x}_S,t) = G(\mathbf{x}_S,\mathbf{x}',t)$, then the right-hand side of equation (17) describes the cross-correlation of responses at receivers at $\mathbf{x}_S$ and $\mathbf{x}$ (both located between $\mathbb{S}_0$ and $\mathbb{S}_1$), due to sources at $\mathbf{x}'$ at the boundaries $\mathbb{S}_0$ and $\mathbb{S}_1$ (Wapenaar & Fokkema 2006). In this form equation (17) is the theoretical basis for Green's function retrieval, also known as seismic interferometry (Weaver & Lobkis 2001; Campillo & Paul 2003; Schuster *et al.* 2004; Snieder 2004; Roux *et al.* 2004; Sabra *et al.* 2007; Draganov *et al.* 2009). Again, a practical limitation is that measurements are often available only at a single boundary. An alternative representation of the homogeneous Green's function, in terms of integrals over a single boundary, follows from the modified version of Huygens' principle in the next section.

MODIFIED HUYGENS' PRINCIPLE, USING FOCUSING FUNCTIONS

In this section we replace the dipole Green's functions in Huygens' principle by focusing functions and, hence, the dipole sources by focal points. In previous work on the Marchenko method we introduced two types of focusing functions: f_1, which has a focal point inside the inhomogeneous medium, and f_2, with its focal point at the boundary between the inhomogeneous lower half-space and the homogeneous upper half-space (Wapenaar *et al.* 2014). Since the dipole Green's functions in Huygens' principle have their sources at the boundary $\mathbb{S}_0$, we choose for focusing functions with their focal points at $\mathbb{S}_0$. Hence, the focusing function we discuss below is akin to the focusing function f_2. However, it is normalized in a different way. Moreover, whereas f_2 is defined in a truncated version of the actual medium, the focusing function we discuss below is defined in the actual medium and it is not decomposed into downgoing and upgoing components inside the medium. Before we discuss the focusing function in an inhomogeneous medium, we start with introducing the focusing function in a homogeneous medium.

Focusing function in a homogeneous medium

We define the focusing function $F(\mathbf{x},\mathbf{x}',t)$ for a homogeneous lossless medium as an upward propagating wave field, of which the wave fronts are half-spheres (in 3D) or half-circles (in 2D) centered at $\mathbf{x}'$ on $\mathbb{S}_0$ (at depth z_0), see Figure 8a for the 2D situation. At negative times, the focusing function propagates (as a function of $\mathbf{x}$ and t) upward through the lower half-space towards $\mathbb{S}_0$, at $t=0$ it focuses at $\mathbf{x}=\mathbf{x}'$ on $\mathbb{S}_0$, and at positive times it propagates upward through the upper half-space away from $\mathbb{S}_0$. In the upper half-space, we relate this focusing function to the dipole Green's function of Figure 2 via

$$F(\mathbf{x},\mathbf{x}',t) = -2G_{\mathrm{d}}(\mathbf{x},\mathbf{x}',t), \tag{18}$$

for $\mathbf{x}$ above $\mathbb{S}_0$. For $\mathbf{x}$ at $\mathbb{S}_0$ (hence, for $z=z'=z_0$) the focusing condition reads

$$F(\mathbf{x},\mathbf{x}',t)|_{z=z'} = \delta(\mathbf{x}_{\mathrm{H}}-\mathbf{x}'_{\mathrm{H}})\delta(t), \tag{19}$$

where $\mathbf{x}_{\mathrm{H}}$ and $\mathbf{x}'_{\mathrm{H}}$ denote the horizontal components of $\mathbf{x}$ and $\mathbf{x}'$, respectively, hence $\mathbf{x}_{\mathrm{H}}=(x,y)$ and $\mathbf{x}'_{\mathrm{H}}=(x',y')$ (in 3D) or $\mathbf{x}_{\mathrm{H}}=x$ and $\mathbf{x}'_{\mathrm{H}}=x'$ (in 2D). In theory evanescent waves can be included (Dukalski *et al.* 2022; Wapenaar *et al.* 2023), but to avoid instability they are usually suppressed. This implies that the delta functions in the right-hand side of equation (19) should be interpreted as band-limited delta functions.

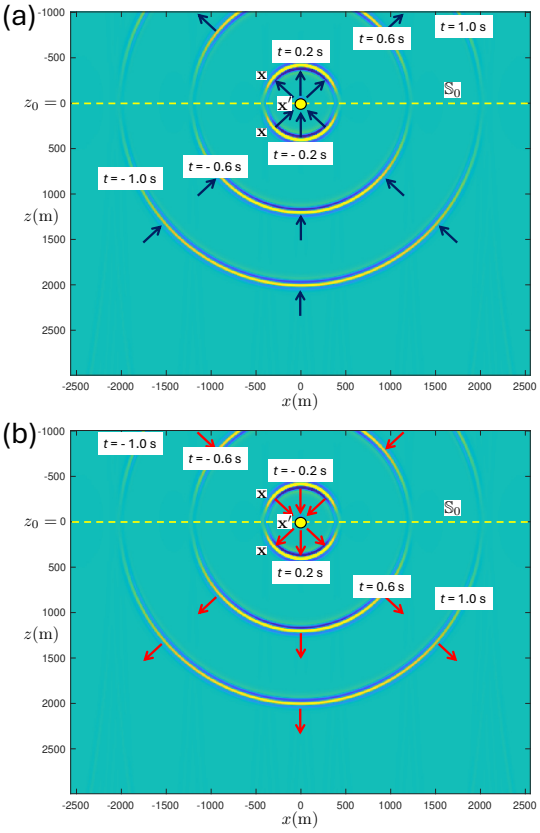

Figure 8. *(a) Focusing function $F(\mathbf{x},\mathbf{x}',t)$ (convolved with a Ricker wavelet to get a nicer display) and (b) its time-reversed version $F(\mathbf{x},\mathbf{x}',-t)$ in a homogeneous medium, for a focal point at $\mathbf{x}'$ on $\mathbb{S}_0$ at depth z_0. Animations at https://www.keeswapenaar.nl/HP2/Movie8a.mp4 and https://www.keeswapenaar.nl/HP2/Movie8b.mp4.*

The time-reversed focusing function $F(\mathbf{x},\mathbf{x}',-t)$, illustrated in Figure 8b for the 2D situation, propagates at negative times downward through the upper half-space towards $\mathbb{S}_0$, at $t=0$ it focuses at $\mathbf{x}=\mathbf{x}'$ on $\mathbb{S}_0$, and at positive times it propagates downward through the lower half-space away from $\mathbb{S}_0$. In the lower half-space, we relate this time-reversed focusing function to the dipole Green's function of Figure 2 via

$$F(\mathbf{x},\mathbf{x}',-t) = 2G_{\mathrm{d}}(\mathbf{x},\mathbf{x}',t), \tag{20}$$

for $\mathbf{x}$ below $\mathbb{S}_0$. Note that, whereas the Green's function $G_{\mathrm{d}}(\mathbf{x},\mathbf{x}',t)$ is the response to a dipole source at $\mathbf{x}'$ on $\mathbb{S}_0$, the focusing function $F(\mathbf{x},\mathbf{x}',t)$ obeys a source-free wave equation (the right-hand side of equation (19) formulates a focusing condition, not a source, see Appendix D for

details). Substituting equation (18) into equation (7) for forward extrapolation of upgoing waves to $\mathbf{x}$ above $\mathbb{S}_0$, or substituting equation (20) into equation (11) for inverse extrapolation of upgoing waves to $\mathbf{x}$ below $\mathbb{S}_0$, we obtain in both cases

$$p^-(\mathbf{x},t) = \int_{\mathbb{S}_0} F(\mathbf{x},\mathbf{x}',t) * p^-(\mathbf{x}',t)\mathrm{d}\mathbf{x}'. \qquad (21)$$

Hence, this expression holds for $\mathbf{x}$ in the upper as well as the lower half-space, as long as $\mathbf{x}$ is above the source in the lower half-space. Similarly, substituting equation (20) into equation (8) for forward extrapolation of downgoing waves to $\mathbf{x}$ below $\mathbb{S}_0$, or substituting equation (18) into equation (12) for inverse extrapolation of downgoing waves to $\mathbf{x}$ above $\mathbb{S}_0$, we obtain in both cases

$$p^+(\mathbf{x},t) = \int_{\mathbb{S}_0} F(\mathbf{x},\mathbf{x}',-t) * p^+(\mathbf{x}',t)\mathrm{d}\mathbf{x}'. \qquad (22)$$

Hence, also this expression holds for $\mathbf{x}$ in the upper and in the lower half-space, as long as $\mathbf{x}$ is below the source in the upper half-space. In absence of sources, equations (21) and (22) hold throughout space.

By introducing the focusing function and its time-reversal, we achieved that the four equations for forward and inverse extrapolation of upgoing and downgoing waves through a homogeneous medium (equations (7), (8), (11) and (12)) are now captured by the two equations (21) and (22). Hence, Figures 1 and 3 can be seen as examples of equation (21) for $\mathbf{x}$ above and below $\mathbb{S}_0$, respectively. For a homogeneous medium there are no further advantages of using the focusing functions instead of the dipole Green's functions. This changes considerably for an inhomogeneous medium.

Focusing function in an inhomogeneous medium

We consider a medium which is inhomogeneous below the boundary $\mathbb{S}_0$ (at depth z_0). At and above this boundary we assume that the medium is homogeneous. For this configuration we define the focusing function $F(\mathbf{x},\mathbf{x}',t)$, with $\mathbf{x}'$ again denoting a focal point at $\mathbb{S}_0$ (hence, $z' = z_0$). Throughout space, $F(\mathbf{x},\mathbf{x}',t)$ obeys the source-free acoustic wave equation, with the condition that at $\mathbb{S}_0$ it obeys the focusing condition, formulated by equation (19), and that at and above $\mathbb{S}_0$ it propagates upward. Hence, at and above $\mathbb{S}_0$ this focusing function is the same as that for a homogeneous medium, discussed in the previous section; below $\mathbb{S}_0$ it is of course different. Assuming the medium is lossless throughout space, the time-reversed focusing function $F(\mathbf{x},\mathbf{x}',-t)$ obeys the same source-free wave equation as $F(\mathbf{x},\mathbf{x}',t)$. At and above $\mathbb{S}_0$ this time-reversed focusing function propagates downward.

We illustrate $F(\mathbf{x},\mathbf{x}',t)$ for the same layered medium as used for previous examples. Figures 9a – 9d show snapshots at times $t = -1.0$ s, $t = -0.6$ s, $t = -0.2$ s and $t = 0.2$ s, respectively. Figures 10a and 10b show cross-sections of $F(\mathbf{x},\mathbf{x}',t)$, and of its time-reversed version $F(\mathbf{x},\mathbf{x}',-t)$, along a vertical line through the focal point, as a function of depth z and time t. The vertical dashed lines in Figure 10a at $t = -1.0$ s, $t = -0.6$ s, $t = -0.2$ s and $t = 0.2$ s correspond to the vertical dashed lines in the snapshots in Figures 9a – 9d. Figures 10c and 10d show ray diagrams of $F(\mathbf{x},\mathbf{x}',t)$ and $F(\mathbf{x},\mathbf{x}',-t)$. From these figures we observe that the focusing function $F(\mathbf{x},\mathbf{x}',t)$ starts with upgoing waves in the half-space below the deepest interface, which are tuned in such a way that, after interaction at the interfaces, a single upgoing wave converges to the focal point (Figures 9c and 10c), focuses at $\mathbf{x} = \mathbf{x}'$ and $t = 0$, and continues as a single upgoing wave, diverging from the focal point (Figure 9d).

Note the different character of the focusing function $F(\mathbf{x},\mathbf{x}',t)$ in Figures 9 and 10 in comparison with the dipole Green's function $G_\mathrm{d}(\mathbf{x},\mathbf{x}',t)$ in Figure 5. Whereas the dipole Green's function obeys a causality condition related to the source at $t = 0$, indicated by the vertical solid line in Figure 5c, the focusing function obeys a focusing condition at z_0, indicated by the horizontal solid lines in Figures 10a and 10b. Conversely, the focusing function is not causal (it exists at negative and positive times, see Figure 10a), whereas the dipole Green's function does not focus at z_0 (it contains multiple upgoing events at z_0, see Figures 5c and 5d).

Modified Huygens' principle

We now discuss how the focusing functions $F(\mathbf{x},\mathbf{x}',t)$ and $F(\mathbf{x},\mathbf{x}',-t)$ can replace the dipole Green's functions $G_\mathrm{d}(\mathbf{x},\mathbf{x}',t)$ and $G_\mathrm{d}(\mathbf{x},\mathbf{x}',-t)$ in Huygens' principle. Recall that we assume that the medium at and above the boundary $\mathbb{S}_0$ is homogeneous. This means that in the upper half-space we can handle downgoing and upgoing waves independent of each other. On the other hand, the medium below $\mathbb{S}_0$ is inhomogeneous. Although in inhomogeneous media, decomposition into downgoing and upgoing waves is often possible locally, in the following analysis we will not make use of this, so in the lower half-space we will only consider the total wave field. For the moment we will assume that the entire medium (above and below $\mathbb{S}_0$) is source-free for the wave field $p(\mathbf{x},t)$ (and for the focusing function it is by definition source-free).

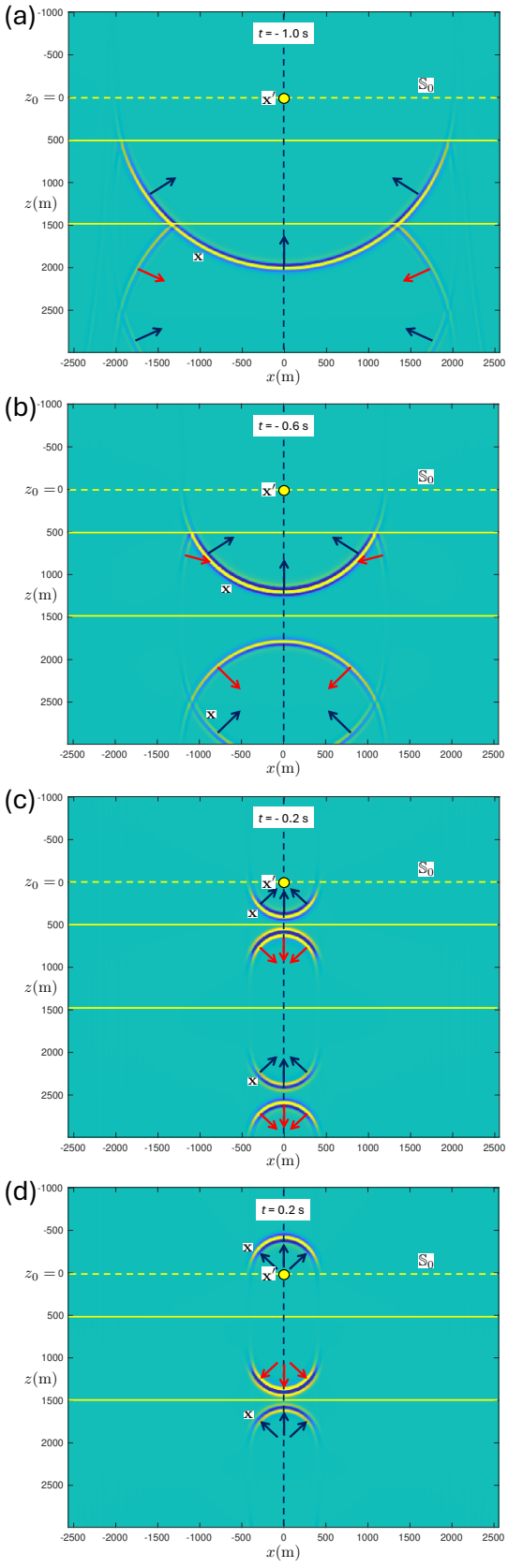

Figure 9. *Focusing function $F(\mathbf{x},\mathbf{x}',t)$ (convolved with a Ricker wavelet) in a layered medium, for a focal point at $\mathbf{x}'$ on $\mathbb{S}_0$ at depth z_0. Animation of $F(\mathbf{x},\mathbf{x}',t)$ at https://www.keeswapenaar.nl/HP2/Movie9a.mp4 and of $F(\mathbf{x},\mathbf{x}',-t)$ at https://www.keeswapenaar.nl/HP2/Movie9b.mp4.*

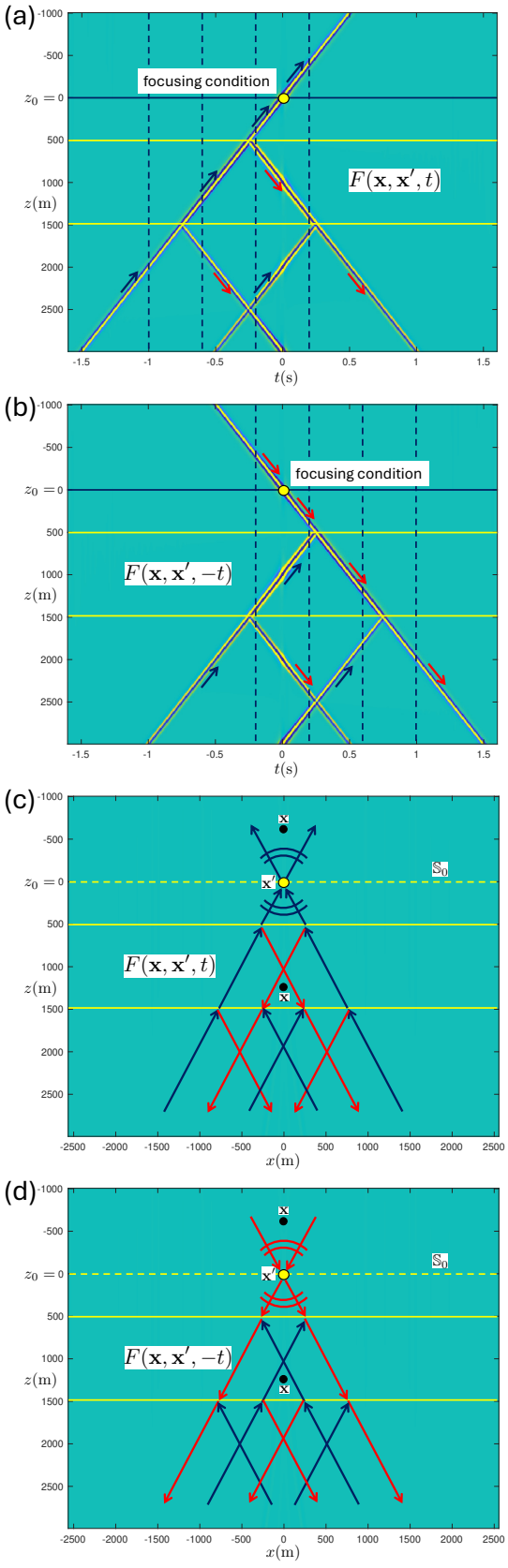

Figure 10. *(a),(b) Cross-sections at $x = x' = 0$ and (c),(d) ray diagrams of the focusing function $F(\mathbf{x},\mathbf{x}',t)$ in Figure 9 and of its time-reversed version $F(\mathbf{x},\mathbf{x}',-t)$.*

In the previous section we remarked that at and above $\mathbb{S}_0$, the focusing function $F(\mathbf{x},\mathbf{x}',t)$ for an inhomogeneous medium is the same as that for a homogeneous medium. Hence, equations (21) and (22), which were derived for $\mathbf{x}$ in the upper and lower half-space in a homogeneous medium, still hold for $\mathbf{x}$ in the homogeneous half-space above $\mathbb{S}_0$, even when the medium below $\mathbb{S}_0$ is inhomogeneous. Defining $p(\mathbf{x},t) = p^-(\mathbf{x},t) + p^+(\mathbf{x},t)$ for $\mathbf{x}$ at and above $\mathbb{S}_0$, we obtain from equations (21) and (22)

$$\begin{aligned} p(\mathbf{x},t) &= \int_{\mathbb{S}_0} F(\mathbf{x},\mathbf{x}',t) * p^-(\mathbf{x}',t)\mathrm{d}\mathbf{x}' \\ &+ \int_{\mathbb{S}_0} F(\mathbf{x},\mathbf{x}',-t) * p^+(\mathbf{x}',t)\mathrm{d}\mathbf{x}'. \end{aligned} \tag{23}$$

From a mathematical viewpoint, this equation describes $p(\mathbf{x},t)$ as a superposition of mutually independent solutions $F(\mathbf{x},\mathbf{x}',t)$ and $F(\mathbf{x},\mathbf{x}',-t)$ of the same source-free wave equation, with $p^-(\mathbf{x}',t)$ and $p^+(\mathbf{x}',t)$ being their coefficients. Although we derived this equation from equations (21) and (22) for $\mathbf{x}$ at and above $\mathbb{S}_0$, the quantities $p(\mathbf{x},t)$, $F(\mathbf{x},\mathbf{x}',t)$ and $F(\mathbf{x},\mathbf{x}',-t)$ all obey the same source-free wave equation for all $\mathbf{x}$ (at, above and below $\mathbb{S}_0$). Hence, if we write $p(\mathbf{x},t)$ for $\mathbf{x}$ below $\mathbb{S}_0$ as a superposition of $F(\mathbf{x},\mathbf{x}',t)$ and $F(\mathbf{x},\mathbf{x}',-t)$, the coefficients must be the same as for $\mathbf{x}$ at and above $\mathbb{S}_0$. In other words, equation (23) holds for all $\mathbf{x}$ throughout space. When there are sources for the wave field $p(\mathbf{x},t)$ in the upper half-space, then equation (23) holds for all $\mathbf{x}$ below the shallowest source (following the same reasoning as for the homogeneous medium). A more formal derivation of equation (23) for all $\mathbf{x}$ below the shallowest source is presented in Appendix D. From this derivation it also follows that evanescent waves are neglected at $\mathbb{S}_0$. This does not mean that evanescent waves are neglected altogether. Waves that are propagating at $\mathbb{S}_0$ may become evanescent in high-velocity layers and equation (23) accounts for such evanescent waves (Wapenaar *et al.* 2021).

Equation (23) formulates the modified Huygens' principle. The two terms on the right-hand side are illustrated in Figure 11, for $\mathbf{x}$ below $\mathbb{S}_0$. First consider Figure 11b. A downgoing wave field $p^+(\mathbf{x}',t)$ is incident from above to the inhomogeneous lower half-space. For each $\mathbf{x}'$ on $\mathbb{S}_0$ it is convolved with the time-reversed focusing function $F(\mathbf{x},\mathbf{x}',-t)$. The integral over all $\mathbf{x}'$ on $\mathbb{S}_0$, as formulated in the second term on the right-hand side of equation (23), extrapolates the field $p^+(\mathbf{x}',t)$ from $\mathbb{S}_0$ into the lower half-space. Since the focusing function implicitly consists of a superposition of downgoing and upgoing waves in the lower half-space (the red and blue rays in Figure 11b), the result of this integral is *not* the forward

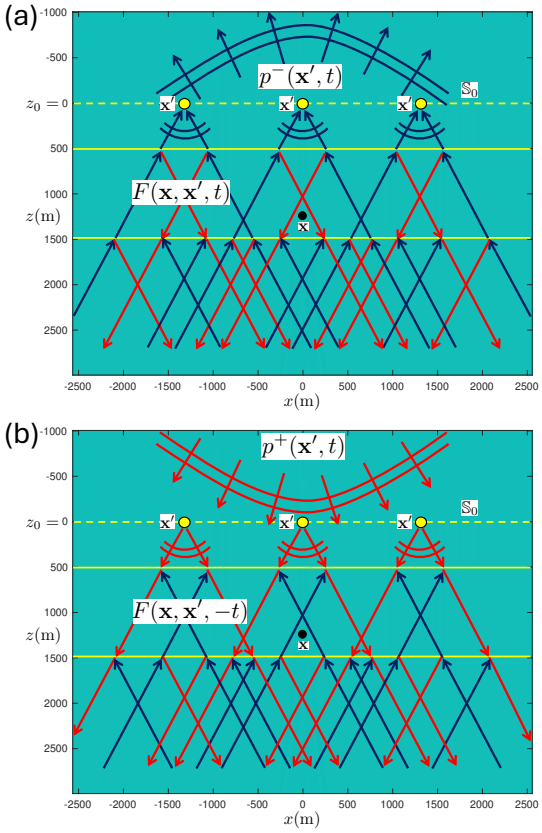

Figure 11. *Ray diagrams of the modified Huygens' principle, as formulated by equation (23). (a) The first and (b) the second term in equation (23).*

extrapolated downgoing field $p^+(\mathbf{x},t)$ in the lower half-space (unlike in the homogeneous medium situation, as formulated by equation (22)). Next, consider Figure 11a. Here the upgoing field $p^-(\mathbf{x}',t)$ is convolved with the focusing function $F(\mathbf{x},\mathbf{x}',t)$ for all $\mathbf{x}'$ on $\mathbb{S}_0$. The integral over all $\mathbf{x}'$ on $\mathbb{S}_0$ (the first term on the right-hand side of equation (23)), extrapolates the field $p^-(\mathbf{x}',t)$ from $\mathbb{S}_0$ into the lower half-space. For similar reasons as above, this is *not* the inverse extrapolated upgoing field $p^-(\mathbf{x},t)$ in the lower half-space. However, the superposition of the two integrals, as formulated by equation (23), yields the total wave field $p(\mathbf{x},t)$ in the lower half-space, including all internal multiple reflections. In comparison with equation (14), where the two integrals are taken over two different boundaries, in equation (23) the two integrals are taken over one and the same boundary. Hence, this makes equation (23) very useful for practical situations in which a medium is often accessible from one side only,

such as in the seismic reflection method. Moreover, it appears that the focusing function can be retrieved from the reflection response, acquired at the same boundary, using the Marchenko method (Broggini & Snieder 2012; Wapenaar *et al.* 2014; Slob *et al.* 2014; Van der Neut *et al.* 2015; Meles *et al.* 2015). In most papers on the Marchenko method it is assumed that the wave field inside the medium can be decomposed into downgoing and upgoing components. This decomposition is avoided in equation (23), which opens the way to handle refracted and evanescent waves (Wapenaar *et al.* 2021; Diekmann & Vasconcelos 2021). A further discussion of the Marchenko method is beyond the scope of this paper. In the next sections we indicate applications of equation (23), assuming the focusing function is known (either from numerical modeling or from applying the Marchenko method to the reflection response).

Simultaneous forward and inverse wave field extrapolation through an inhomogeneous medium

Since equation (23) yields the total wave field in the inhomogeneous half-space below $\mathbb{S}_0$ from downgoing and upgoing waves at $\mathbb{S}_0$, we can interpret it as an expression for simultaneous forward and inverse wave field extrapolation. We illustrate this for the situation of reflection measurements at the boundary $\mathbb{S}_0$. We define the reflection response $R(\mathbf{x}', \mathbf{x}'', t)$ of the inhomogeneous lower half-space via the relation

$$p^-(\mathbf{x}', t) = \int_{\mathbb{S}_0} R(\mathbf{x}', \mathbf{x}'', t) * p^+(\mathbf{x}'', t) \mathrm{d}\mathbf{x}'', \qquad (24)$$

for $\mathbf{x}'$ and $\mathbf{x}''$ at $\mathbb{S}_0$. We consider a dipole source in the homogeneous upper half-space at $\mathbf{x}_D = (\mathbf{x}_{\mathrm{H},D}, z_0 - \epsilon)$ (with $\mathbf{x}_{\mathrm{H},D}$ denoting the horizontal component(s) of $\mathbf{x}_D$), at a vanishing distance ϵ above $\mathbb{S}_0$. This is the source for the wave field $p(\mathbf{x}, t)$. We scale it such that for the downgoing field for $\mathbf{x}''$ at $\mathbb{S}_0$ we have

$$p^+(\mathbf{x}'', t) = \delta(\mathbf{x}''_H - \mathbf{x}_{\mathrm{H},D}) s(t), \qquad (25)$$

where $s(t)$ is the source wavelet. Substitution of equation (25) into equation (24) gives

$$p^-(\mathbf{x}', t) = R(\mathbf{x}', \mathbf{x}_D, t) * s(t), \qquad (26)$$

for $\mathbf{x}'$ at $\mathbb{S}_0$. Substitution of equations (25) and (26) into equation (23) yields

$$\begin{aligned} p(\mathbf{x}, t) \quad = \quad & \int_{\mathbb{S}_0} F(\mathbf{x}, \mathbf{x}', t) * R(\mathbf{x}', \mathbf{x}_D, t) * s(t) \mathrm{d}\mathbf{x}' \\ & + F(\mathbf{x}, \mathbf{x}_D, -t) * s(t). \end{aligned} \qquad (27)$$

Since the source at $\mathbf{x}_D$ lies just above $\mathbb{S}_0$, this expression holds only for $\mathbf{x}$ at and below $\mathbb{S}_0$. First we evaluate a discretized version of only the first term on the right-hand side of equation (27), i.e.,

$$\sum_{n=-N}^{N} F(\mathbf{x}, \mathbf{x}_n, t) * R(\mathbf{x}_n, \mathbf{x}_D, t) * s(t), \qquad (28)$$

with $\mathbf{x}_n = (n\Delta x, z_0)$, $\Delta x = 200$ m and $N = 50$. For this 2D example we choose $\mathbf{x}_{\mathrm{H},D} = x_D = 0$. The result is shown in Figures 12a–12d, for $t = 0.2$ s, $t = 0.6$ s, $t = 1.0$ s, and $t = 1.4$ s, respectively. The envelopes of the superposed waves converge to wave fronts, but it is not yet clear how they are connected to the desired response $p(\mathbf{x}, t)$ (which is the response to a dipole source at $\mathbf{x}_D$). Next, we replace the summation by an integration and we add the term $F(\mathbf{x}, \mathbf{x}_D, -t) * s(t)$, i.e., we add Figures 9c, 9b and 9a to the converged versions of Figures 12a, 12b and 12c. The results are shown in Figure 13. This figure clearly shows the desired response to the dipole source at $\mathbf{x}_D$, observed at all $\mathbf{x}$ in the lower half-space, including internal multiple reflections (compare Figures 13a and 13d with the directly modeled dipole Green's function in the lower half-space in Figures 5a and 5b at $t = 0.2$ s and $t = 1.4$ s, respectively).

Extrapolation of reflection data with focusing functions finds applications in acoustic and seismic imaging schemes, accounting for internal multiple reflections (Ravasi *et al.* 2016; Jia *et al.* 2018; Staring & Wapenaar 2020; Brackenhoff *et al.* 2022). In those applications the focusing functions are obtained with the Marchenko method.

Retrieval of the homogeneous Green's function in an inhomogeneous medium

In equation (16) we introduced the homogeneous Green's function $G_{\mathrm{h}}(\mathbf{x}, \mathbf{x}_S, t) = G(\mathbf{x}, \mathbf{x}_S, t) + G(\mathbf{x}, \mathbf{x}_S, -t)$ for an inhomogeneous lossless medium. Both terms on the right-hand side obey a wave equation with a source at $\mathbf{x}_S$, but these sources cancel each other, implying that the wave equation for $G_{\mathrm{h}}(\mathbf{x}, \mathbf{x}_S, t)$ is source-free, see Appendix A-2. Hence, if in equation (23) we replace $p(\mathbf{x}, t)$ by $G_{\mathrm{h}}(\mathbf{x}, \mathbf{x}_S, t)$, it will hold throughout space, independent of the position of $\mathbf{x}_S$. With this replacement, the upgoing and downgoing wave fields $p^-(\mathbf{x}', t)$ and $p^+(\mathbf{x}', t)$ on the right-hand side of equation (23) need to be replaced by $G^-_{\mathrm{h}}(\mathbf{x}', \mathbf{x}_S, t)$ and $G^+_{\mathrm{h}}(\mathbf{x}', \mathbf{x}_S, t)$, respectively. Assuming again that $\mathbf{x}_S$ lies below $\mathbb{S}_0$, taking into account that $\mathbf{x}'$ is situated at $\mathbb{S}_0$ and that the half-space

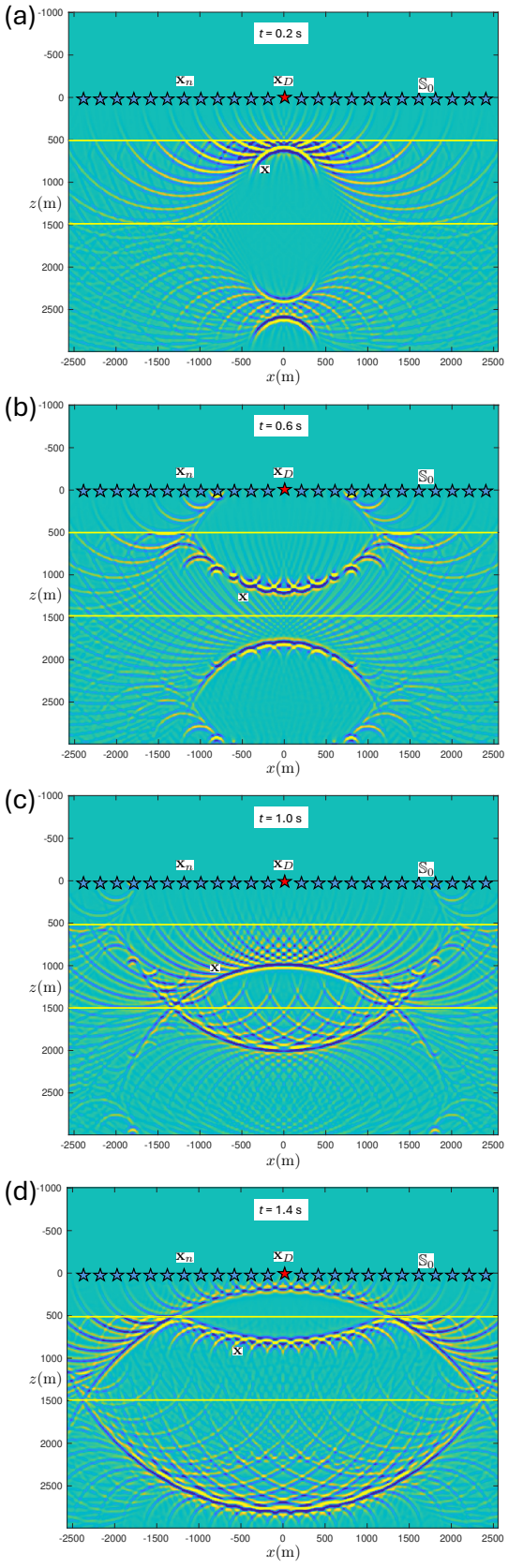

Figure 12. *Illustration of the first term of the modified Huygens' principle (equation (28)), applied to the discretized reflection response* $R(\mathbf{x}_n, \mathbf{x}_D, t) * s(t)$. *Animations at https://www.keeswapenaar.nl/HP2/Movie12a.mp4 and https://www.keeswapenaar.nl/HP2/Movie12b.mp4.*

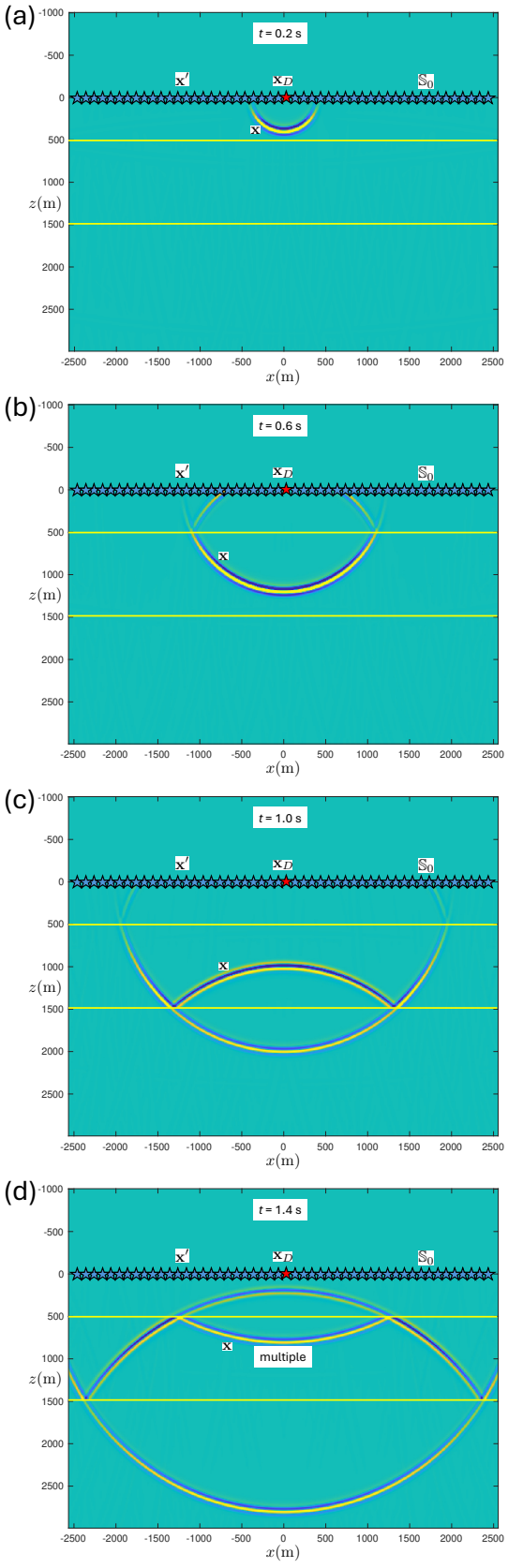

Figure 13. *Illustration of the modified Huygens' principle (both terms of equation (27)), applied to the continuous reflection response* $R(\mathbf{x}', \mathbf{x}_D, t) * s(t)$. *Animation at https://www.keeswapenaar.nl/HP2/Movie13.mp4.*

above $\mathbb{S}_0$ is homogeneous, it follows that the Green's function $G(\mathbf{x}', \mathbf{x}_S, t)$ propagates upward for $\mathbf{x}'$ at $\mathbb{S}_0$ (see Figure 4). As a result, the time-reversed Green's function $G(\mathbf{x}', \mathbf{x}_S, -t)$ propagates downward for $\mathbf{x}'$ at $\mathbb{S}_0$. Since these two terms consitute the total homogeneous Green's function, it follows that $G_{\rm h}^{-}(\mathbf{x}', \mathbf{x}_S, t) = G(\mathbf{x}', \mathbf{x}_S, t)$ and $G_{\rm h}^{+}(\mathbf{x}', \mathbf{x}_S, t) = G(\mathbf{x}', \mathbf{x}_S, -t)$ for $\mathbf{x}'$ at $\mathbb{S}_0$. With these substitutions, equation (23) becomes

$$\begin{aligned} G_{\rm h}(\mathbf{x}, \mathbf{x}_S, t) &= \int_{\mathbb{S}_0} F(\mathbf{x}, \mathbf{x}', t) * G(\mathbf{x}', \mathbf{x}_S, t) {\rm d}\mathbf{x}' \\ &+ \int_{\mathbb{S}_0} F(\mathbf{x}, \mathbf{x}', -t) * G(\mathbf{x}', \mathbf{x}_S, -t) {\rm d}\mathbf{x}', \end{aligned} \tag{29}$$

for all $\mathbf{x}$ throughout space. Compare this with equation (17), where the two integrals are taken over two different boundaries. In equation (29) both integrals are taken over the same boundary. Moreover, the second integral is merely the time-reversal of the first integral.

We illustrate equation (29) for the same layered medium as in the previous examples and with $\mathbf{x}_S = (0, 1200)$ m. First we evaluate a discretized version of only the first term on the right-hand side of equation (29), i.e.,

$$\sum_{n=-N}^{N} F(\mathbf{x}, \mathbf{x}_n, t) * G(\mathbf{x}_n, \mathbf{x}_S, t), \tag{30}$$

with $\mathbf{x}_n = (n\Delta x, z_0)$, $\Delta x = 200$ m, $N = 50$, and with $G(\mathbf{x}_n, \mathbf{x}_S, t)$ tapered at large propagation angles. The result is shown in Figures 14a–14d, for $t = 0.8$ s, $t = 0.4$ s, $t = 0.0$ s, and $t = -0.4$ s, respectively. Next, we replace the summation by an integration and we add its time-reversal, i.e., we superpose the converged versions of Figures 14b and 14d, etc. The result is shown in Figure 15. This figure shows the retrieved homogeneous Green's function $G_{\rm h}(\mathbf{x}, \mathbf{x}_S, t)$. Note that the result in Figure 15 is indistinguishable from that in Figure 7. However, whereas Figure 7 was obtained from an integral over two boundaries, using the traditional Huygens' principle with time-reversed dipole Green's functions, Figure 15 is the result of an integral over a single boundary and its time-reversal, using the modified Huygens' principle with focusing functions.

Retrieval of the homogeneous Green's function from observations at a single boundary finds applications in holographic imaging and inverse scattering (Wapenaar *et al.* 2016; Diekmann & Vasconcelos 2021) and in monitoring of induced acoustic (Van der Neut *et al.* 2017) and seismic sources (Brackenhoff *et al.* 2019). Also in those applications the focusing functions are obtained from the reflection response with the Marchenko method.

CONCLUSIONS

Huygens' principle stands as a milestone in the history of wave theory. Originally formulated to explain propagation, diffraction and interference of light, it has found many applications in optics, acoustics, geophysics, etc. Central in the mathematical formulation of Huygens' principle, due to 19th century physicists Kirchhoff, Helmholtz, Rayleigh and others, is the Green's function, which formalizes the responses to the secondary sources in Huygens' principle. Many of present-day applications of Huygens' principle use time-reversed Green's functions. These time-reversed Green's functions are acausal and as such do not describe physical responses to secondary sources. However, they play a fundamental role in algorithms for backpropagation, imaging, inversion, seismic interferometry, etc.

We have demonstrated with numerical examples that the traditional Huygens' principle with time-reversed Green's functions has limitations when the medium is inhomogeneous. In particular, when measurements are available only at a single boundary, internal multiples are incorrectly handled. To remedy this, Huygens' principle has been modified by replacing the Green's functions by focusing functions. For a homogeneous medium this replacement does not make much difference, but for an inhomogeneous medium the difference is considerable. Using the modified Huygens' principle with focusing functions, the limitations of the traditional Huygens' principle with time-reversed Green's functions are evaded. This has been explained with numerical examples for a simple horizontally layered medium, but note that the modified principle holds for an arbitrary inhomogeneous medium. The only assumption is that evanescent waves can be ignored at the boundary between the inhomogeneous lower half-space and the homogeneous upper half-space. No assumptions are made about up-down decomposition inside the inhomogeneous lower half-space.

Similar as the time-reversed Green's functions, the focusing functions do not describe physical responses to secondary sources. However, they play an important role in novel algorithms for acoustic and seismic imaging and inverse scattering, for monitoring of induced acoustic and seismic sources, etc. In all these cases, the focusing functions can be obtained from the reflection response with the Marchenko method and internal multiple reflections are properly taken into account.

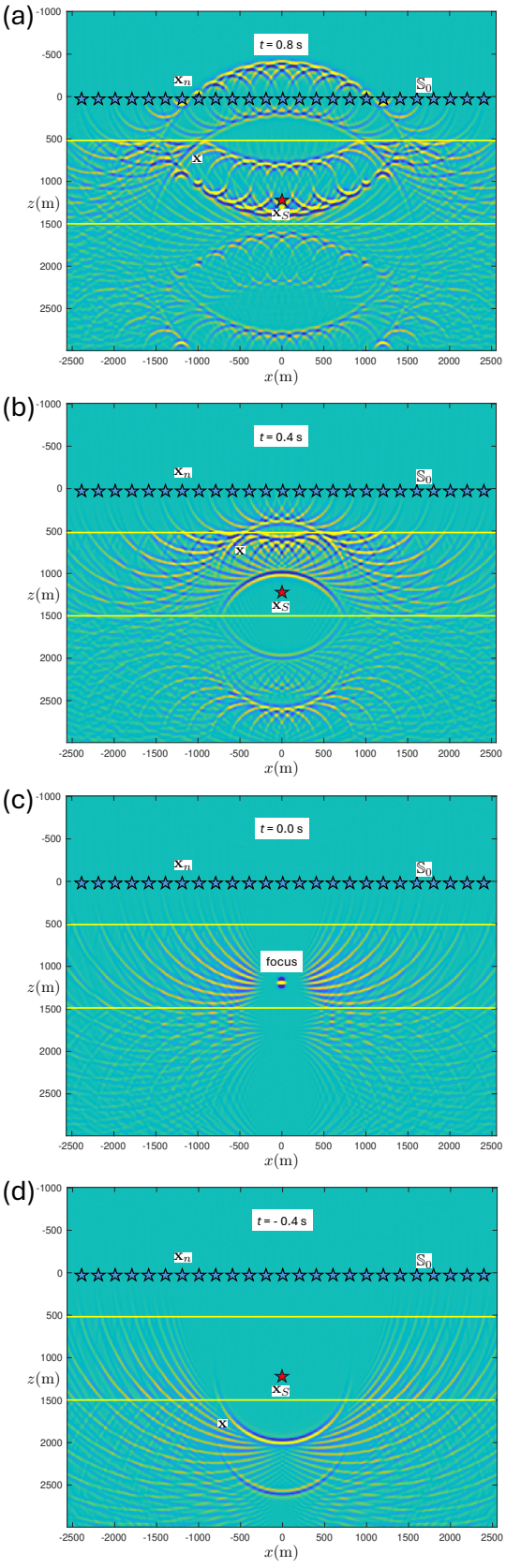

Figure 14. *Illustration of the first term of the modified Huygens' principle (equation (30)), applied to the discretized Green's function $G(\mathbf{x}_n, \mathbf{x}_S, t)$. Animations at https://www.keeswapenaar.nl/HP2/Movie14a.mp4 and https://www.keeswapenaar.nl/HP2/Movie14b.mp4.*

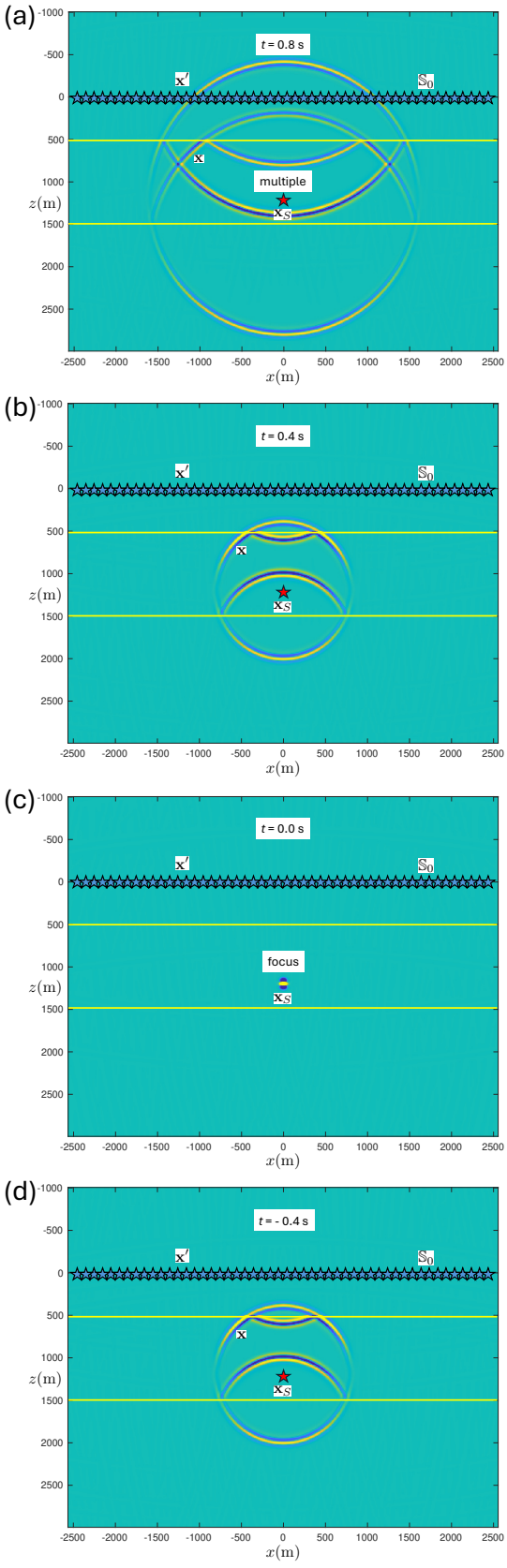

Figure 15. *Illustration of the modified Huygens' principle (both terms of equation (29)), applied to the continuous Green's function $G(\mathbf{x}', \mathbf{x}_S, t)$ and its time-reversal $G(\mathbf{x}', \mathbf{x}_S, -t)$. Animation at https://www.keeswapenaar.nl/HP2/Movie15.mp4.*

REFERENCES

Berkhout, A. J., 1985. *Seismic Migration. Imaging of acoustic energy by wave field extrapolation. A. Theoretical aspects (3rd edition)*, Elsevier, Amsterdam.

Berkhout, A. J. & Wapenaar, C. P. A., 1989. One-way versions of the Kirchhoff integral, *Geophysics*, **54**(4), 460–467.

Bleistein, N., 1984. *Mathematical methods for wave phenomena*, Academic Press, Inc., Orlando.

Bojarski, N. N., 1983. Generalized reaction principles and reciprocity theorems for the wave equations and the relationship between the time-advanced and time-retarded fields, *Journal of the Acoustical Society of America*, **74**, 281–285.

Brackenhoff, J., Thorbecke, J., & Wapenaar, K., 2019. Monitoring of induced distributed double-couple sources using Marchenko-based virtual receivers, *Solid Earth*, **10**, 1301–1319.

Brackenhoff, J., Thorbecke, J., Meles, G., Koehne, V., Barrera, D., & Wapenaar, K., 2022. 3D Marchenko applications: implementation and examples, *Geophysical Prospecting*, **70**, 35–56.

Broggini, F. & Snieder, R., 2012. Connection of scattering principles: a visual and mathematical tour, *European Journal of Physics*, **33**, 593–613.

Campillo, M. & Paul, A., 2003. Long-range correlations in the diffuse seismic coda, *Science*, **299**, 547–549.

Cohen, J. K., Hagin, F. G., & Bleistein, N., 1986. Three-dimensional Born inversion with an arbitrary reference, *Geophysics*, **51**, 1552–1558.

Corones, J. P., 1975. Bremmer series that correct parabolic approximations, *J. Math. Anal. Appl.*, **50**, 361–372.

Diekmann, L. & Vasconcelos, I., 2021. Focusing and Green's function retrieval in three-dimensional inverse scattering revisited: A single-sided Marchenko integral for the full wave field, *Physical Review Research*, **3**, 013206.

Draganov, D., Campman, X., Thorbecke, J., Verdel, A., & Wapenaar, K., 2009. Reflection images from ambient seismic noise, *Geophysics*, **74**(5), A63–A67.

Dukalski, M., Reinicke, C., & Wapenaar, K., 2022. Implications of evanescent waves for the Marchenko method through the lens of the transfer-scattering matrix relation, in *EAGE, Extended Abstracts*, pp. 1–4.

Fink, M., 1992. Time-reversal of ultrasonic fields: Basic principles, *IEEE Transactions on Ultrasonics, Ferroelectrics and Frequency Control*, **39**, 555–566.

Fishman, L & McCoy, J J, 1984. Derivation and application of extended parabolic wave theories. I. The factorized Helmholtz equation, *J. Math. Phys.*, **25**(2), 285–296.

Frazer, L. N. & Sen, M. K., 1985. Kirchhoff-Helmholtz reflection seismograms in a laterally inhomogeneous multi-layered elastic medium, I, Theory, *Geophysical Journal of the Royal Astronomical Society*, **80**, 121–147.

Gazdag, J., 1978. Wave equation migration with the phase-shift method, *Geophysics*, **43**, 1342–1351.

Jia, X., Guitton, A., & Snieder, R., 2018. A practical implementation of subsalt Marchenko imaging with a Gulf of Mexico data set, *Geophysics*, **83**(5), S409–S419.

McMechan, G. A., 1983. Migration by extrapolation of time-dependent boundary values, *Geophysical Prospecting*, **31**, 413–420.

Meles, G. A., Löer, K., Ravasi, M., Curtis, A., & da Costa Filho, C. A., 2015. Internal multiple prediction and removal using Marchenko autofocusing and seismic interferometry, *Geophysics*, **80**(1), A7–A11.

Morse, P. M. & Feshbach, H., 1953. *Methods of theoretical physics, Vol. I*, McGraw-Hill Book Company Inc., New York.

Moser, T. J. & Robinson, E. A., 2024. *Walking with Christiaan Huygens. From Archimedes' influence to unsung contributions in modern science*, Springer.

Oristaglio, M. L., 1989. An inverse scattering formula that uses all the data, *Inverse Problems*, **5**, 1097–1105.

Porter, R. P., 1970. Diffraction-limited, scalar image formation with holograms of arbitrary shape, *Journal of the Optical Society of America*, **60**, 1051–1059.

Ravasi, M., Vasconcelos, I., Kritski, A., Curtis, A., da Costa Filho, C. A., & Meles, G. A., 2016. Target-oriented Marchenko imaging of a North Sea field, *Geophysical Journal International*, **205**, 99–104.

Rayleigh, J. W. S., 1878. *The theory of sound. Volume II*, Dover Publications, Inc. (Reprint 1945).

Roux, P., Kuperman, W. A., & the NPAL Group, 2004. Extracting coherent wave fronts from acoustic ambient noise in the ocean, *Journal of the Acoustical Society of America*, **116**, 1995–2003.

Sabra, K. G., Conti, S., Roux, P., & Kuperman, W. A., 2007. Passive *in vivo* elastography from skeletal muscle noise, *Applied Physics Letters*, **90**, 194101.

Schneider, W. A., 1978. Integral formulation for migration in two and three dimensions, *Geophysics*, **43**, 49–76.

Schuster, G. T., Yu, J., Sheng, J., & Rickett, J., 2004. Interferometric/daylight seismic imaging, *Geophysical Journal International*, **157**, 838–852.

Slob, E., Wapenaar, K., Broggini, F., & Snieder, R., 2014. Seismic reflector imaging using internal multiples with Marchenko-type equations, *Geophysics*, **79**(2), S63–S76.

Snieder, R., 2004. Extracting the Green's function from the correlation of coda waves: A derivation based on stationary phase, *Physical Review E*, **69**, 046610.

Staring, M. & Wapenaar, K., 2020. Three-dimensional Marchenko internal multiple attenuation on narrow azimuth streamer data of the Santos Basin, Brazil, *Geophysical Prospecting*, **68**, 1864–1877.

Tygel, M., Schleicher, J., Santos, L. T., & Hubral, P., 2000. An asymptotic inverse to the Kirchhoff-Helmholtz integral, *Inverse Problems*, **16**, 425–445.

Ursin, B., 1983. Review of elastic and electromagnetic wave propagation in horizontally layered media, *Geophysics*, **48**, 1063–1081.

Van der Neut, J., Vasconcelos, I., & Wapenaar, K., 2015. On Green's function retrieval by iterative substitution of the coupled Marchenko equations, *Geophysical Journal International*, **203**, 792–813.

Van der Neut, J., Johnson, J. L., van Wijk, K., Singh, S.,

Slob, E., & Wapenaar, K., 2017. A Marchenko equation for acoustic inverse source problems, *Journal of the Acoustical Society of America*, **141**(6), 4332–4346.

Wapenaar, C. P. A., Peels, G. L., Budejicky, V., & Berkhout, A. J., 1989. Inverse extrapolation of primary seismic waves, *Geophysics*, **54**(7), 853–863.

Wapenaar, K. & Fokkema, J., 2006. Green's function representations for seismic interferometry, *Geophysics*, **71**(4), SI33–SI46.

Wapenaar, K., Thorbecke, J., van der Neut, J., Broggini, F., Slob, E., & Snieder, R., 2014. Marchenko imaging, *Geophysics*, **79**(3), WA39–WA57.

Wapenaar, K., van der Neut, J., & Slob, E., 2016. Unified double- and single-sided homogeneous Green's function representations, *Proceedings of the Royal Society A*, **472**, 20160162.

Wapenaar, K., Snieder, R., de Ridder, S., & Slob, E., 2021. Green's function representations for Marchenko imaging without up/down decomposition, *Geophysical Journal International*, **227**, 184–203.

Wapenaar, K., Dukalski, M., Reinicke, C., & Snieder, R., 2023. Propagator and transfer matrices, Marchenko focusing functions and their mutual relations, *Geophysical Journal International*, **235**, 1403–1419.

Weaver, R. L. & Lobkis, O. I., 2001. Ultrasonics without a source: Thermal fluctuation correlations at MHz frequencies, *Physical Review Letters*, **87**, 134301.

Whitmore, N. D., 1983. Iterative depth migration by backward time propagation, in *SEG, Expanded Abstracts*, pp. 382–385.

APPENDIX A: MONOPOLE AND DIPOLE GREEN'S FUNCTIONS

A–1: Monopole Green's function

The wave equation for the acoustic pressure $p(\mathbf{x},t)$ in an inhomogeneous lossless medium with propagation velocity $c(\mathbf{x})$ and mass density $\rho(\mathbf{x})$ reads

$$\mathcal{L}p = -\partial_t q, \qquad (A\text{–}1)$$

with ∂_t standing for $\partial/\partial t$, wave operator $\mathcal{L}(\mathbf{x},t)$ defined as

$$\mathcal{L} = \nabla\cdot\frac{1}{\rho}\nabla - \frac{1}{\rho c^2}\partial_t^2 \qquad (A\text{–}2)$$

and source function $q(\mathbf{x},t)$ being the volume-injection rate density. We define the Green's function $\mathcal{G}(\mathbf{x},\mathbf{x}',t)$ as the solution of

$$\mathcal{L}\mathcal{G} = -\delta(\mathbf{x}-\mathbf{x}')\delta(t), \qquad (A\text{–}3)$$

with $\delta(\mathbf{x}) = \delta(x)\delta(y)\delta(z)$ and causality condition

$$\mathcal{G}(\mathbf{x},\mathbf{x}',t) = 0, \quad \text{for} \quad t<0. \qquad (A\text{–}4)$$

Hence, $\mathcal{G}(\mathbf{x},\mathbf{x}',t)$ is the response to an impulse at $\mathbf{x}'$ and $t=0$, observed at $\mathbf{x}$ as a function of t. Similarly, we define $G(\mathbf{x},\mathbf{x}',t)$ as the response to an impulsive volume-injection rate source $q(\mathbf{x},t) = \delta(\mathbf{x}-\mathbf{x}')\delta(t)$, hence, it obeys

$$\mathcal{L}G = -\delta(\mathbf{x}-\mathbf{x}')\partial_t\delta(t) \qquad (A\text{–}5)$$

and a causality condition similar to equation $(A\text{–}4)$. We apply the operator ∂_t to both sides of equation $(A\text{–}3)$ and use the property $\partial_t\mathcal{L} = \mathcal{L}\partial_t$ (since $\rho(\mathbf{x})$ and $c(\mathbf{x})$ are independent of t). Comparing the result with equation $(A\text{–}5)$, it follows that $G(\mathbf{x},\mathbf{x}',t)$ and $\mathcal{G}(\mathbf{x},\mathbf{x}',t)$ are mutually related via

$$G(\mathbf{x},\mathbf{x}',t) = \partial_t\mathcal{G}(\mathbf{x},\mathbf{x}',t). \qquad (A\text{–}6)$$

Note that the source terms in equations $(A\text{–}3)$ and $(A\text{–}5)$ represent monopole sources at $\mathbf{x}'$, hence, we call G and $\mathcal{G}$ monopole Green's functions.

For the special case of a homogeneous medium we have for the 3D situation

$$\mathcal{G}(\mathbf{x},\mathbf{x}',t) = \rho\frac{\delta(t-|\mathbf{x}-\mathbf{x}'|/c)}{4\pi|\mathbf{x}-\mathbf{x}'|} \qquad (A\text{–}7)$$

and for the 2D situation

$$\mathcal{G}(\mathbf{x},\mathbf{x}',t) = \rho\frac{H(t-|\mathbf{x}-\mathbf{x}'|/c)}{2\pi\sqrt{t^2-|\mathbf{x}-\mathbf{x}'|^2/c^2}}, \qquad (A\text{–}8)$$

where $H(t)$ is the Heaviside function. According to equation $(A\text{-}6)$, explicit expressions for $G(\mathbf{x},\mathbf{x}',t)$ in a homogeneous medium are obtained by taking the time-derivative of the expressions in the right-hand sides of equations $(A\text{-}7)$ and $(A\text{-}8)$.

A–2: Homogeneous Green's function

We consider again an inhomogeneous lossless medium, with propagation velocity $c(\mathbf{x})$ and mass density $\rho(\mathbf{x})$. Since operator $\mathcal{L}$, defined in equation $(A\text{-}2)$, contains only even order time-derivatives and the source term in wave equation $(A\text{-}3)$ is an even function of time, the time-reversed Green's function $\mathcal{G}(\mathbf{x},\mathbf{x}',-t)$ also obeys this wave equation. We define the homogeneous Green's function $\mathcal{G}_{\rm h}(\mathbf{x},\mathbf{x}',t)$ as

$$\mathcal{G}_{\rm h}(\mathbf{x},\mathbf{x}',t) = \mathcal{G}(\mathbf{x},\mathbf{x}',t) - \mathcal{G}(\mathbf{x},\mathbf{x}',-t) \qquad (A\text{–}9)$$

(Porter 1970; Oristaglio 1989). Since equation $(A\text{-}3)$ holds for both terms in the right-hand side, their difference obeys the homogeneous differential equation $\mathcal{L}\mathcal{G}_{\rm h} = 0$ (hence the name "homogeneous Green's function" for $\mathcal{G}_{\rm h}$).

Since the source term in wave equation $(A\text{-}5)$ is an odd function of time, the opposite time-reversed Green's

function $-G(\mathbf{x},\mathbf{x}',-t)$ also obeys this wave equation. Hence, the homogeneous Green's function $G_{\rm h}(\mathbf{x},\mathbf{x}',t)$, defined as

$$G_{\rm h}(\mathbf{x},\mathbf{x}',t) = G(\mathbf{x},\mathbf{x}',t) + G(\mathbf{x},\mathbf{x}',-t), \qquad (A\text{–}10)$$

obeys the homogeneous differential equation $\mathcal{L}G_{\rm h} = 0$. From equation (A-6) and the definitions of $\mathcal{G}_{\rm h}$ and $G_{\rm h}$, it follows that these homogeneous Green's functions are mutually related via

$$G_{\rm h}(\mathbf{x},\mathbf{x}',t) = \partial_t \mathcal{G}_{\rm h}(\mathbf{x},\mathbf{x}',t). \qquad (A\text{–}11)$$

A–3: Dipole Green's function

Next, we define a Green's function $G_{\rm d}(\mathbf{x},\mathbf{x}',t)$ as the solution of

$$\mathcal{L}G_{\rm d} = \frac{1}{\rho(\mathbf{x}')}\partial_z \delta(\mathbf{x}-\mathbf{x}')\delta(t), \qquad (A\text{–}12)$$

with a causality condition similar to equation (A–4), and ∂_z standing for $\partial/\partial z$. Note that

$$\partial_z \delta(z-z') = \lim_{\Delta z\to 0} \frac{\delta(z+\frac{\Delta z}{2}-z') - \delta(z-\frac{\Delta z}{2}-z')}{\Delta z}, \qquad (A\text{–}13)$$

hence, the right-hand side of equation (A–12) represents a vertically oriented dipole source at $\mathbf{x}'$. Therefore we call $G_{\rm d}$ a dipole Green's function. We define ∂'_z as an operator for differentiation with respect to z'. We apply this operator to both sides of equation (A–3) and use the properties $\partial'_z\mathcal{L} = \mathcal{L}\partial'_z$ (since $\rho(\mathbf{x})$ and $c(\mathbf{x})$ are independent of z') and $\partial'_z\delta(z-z') = -\partial_z\delta(z-z')$. Comparing the result with equation (A–12), it follows that $G_{\rm d}(\mathbf{x},\mathbf{x}',t)$ and $\mathcal{G}(\mathbf{x},\mathbf{x}',t)$ are mutually related via

$$G_{\rm d}(\mathbf{x},\mathbf{x}',t) = \frac{1}{\rho(\mathbf{x}')}\partial'_z \mathcal{G}(\mathbf{x},\mathbf{x}',t). \qquad (A\text{–}14)$$

APPENDIX B: FORWARD WAVE FIELD EXTRAPOLATION

We define the temporal Fourier transform of a space- and time-dependent quantity $p(\mathbf{x},t)$ as

$$\hat{p}(\mathbf{x},\omega) = \int_{-\infty}^{\infty} p(\mathbf{x},t)\exp(i\omega t){\rm d}t, \qquad (B\text{–}1)$$

where i is the imaginary unit and ω the angular frequency (we consider positive ω only). With this definition, differentiation with respect to t in the time domain is replaced by multiplication with $-i\omega$ in the frequency domain, hence, wave equations (A–1) and (A–3) transform to

$$\hat{\mathcal{L}}\hat{p} = i\omega\hat{q} \qquad (B\text{–}2)$$

and

$$\hat{\mathcal{L}}\hat{\mathcal{G}} = -\delta(\mathbf{x}-\mathbf{x}'), \qquad (B\text{–}3)$$

respectively, with operator $\hat{\mathcal{L}}(\mathbf{x},\omega)$ defined as

$$\hat{\mathcal{L}} = \nabla\cdot\frac{1}{\rho}\nabla + \frac{\omega^2}{\rho c^2}. \qquad (B\text{–}4)$$

Consider the quantity $\nabla\cdot\{\hat{\mathcal{G}}(\frac{1}{\rho}\nabla\hat{p}) - \hat{p}(\frac{1}{\rho}\nabla\hat{\mathcal{G}})\}$, apply the product rule for differentiation and simplify the result using wave equations (B–2) and (B–3). This yields

$$\nabla\cdot\{\hat{\mathcal{G}}\frac{1}{\rho}\nabla\hat{p} - \hat{p}\frac{1}{\rho}\nabla\hat{\mathcal{G}}\} = i\omega\hat{\mathcal{G}}\hat{q} + \hat{p}\delta(\mathbf{x}-\mathbf{x}'). \qquad (B\text{–}5)$$

Integrate both sides of this equation over a domain $\mathbb{V}$ with boundary $\mathbb{S}$ and outward pointing normal vector $\mathbf{n}$ and apply the theorem of Gauss to the left-hand side. Use the source-receiver reciprocity relation $\hat{\mathcal{G}}(\mathbf{x},\mathbf{x}',\omega) = \hat{\mathcal{G}}(\mathbf{x}',\mathbf{x},\omega)$ and subsequently modify the notation by replacing all $\mathbf{x}$ by $\mathbf{x}'$ and vice-versa (meaning that effectively $\hat{\mathcal{G}}(\mathbf{x},\mathbf{x}',\omega)$ remains unchanged). This yields the Kirchhoff-Helmholtz integral representation (Morse & Feshbach 1953; Bleistein 1984)

$$\begin{aligned}\chi_{\mathbb{V}}(\mathbf{x})\hat{p}(\mathbf{x},\omega) &= -\int_{\mathbb{V}} i\omega\hat{\mathcal{G}}(\mathbf{x},\mathbf{x}',\omega)\hat{q}(\mathbf{x}',\omega){\rm d}\mathbf{x}' \\ &+ \oint_{\mathbb{S}} \frac{1}{\rho(\mathbf{x}')}\Big(\hat{\mathcal{G}}(\mathbf{x},\mathbf{x}',\omega)\nabla'\hat{p}(\mathbf{x}',\omega) \\ &- \hat{p}(\mathbf{x}',\omega)\nabla'\hat{\mathcal{G}}(\mathbf{x},\mathbf{x}',\omega)\Big)\cdot\mathbf{n}{\rm d}\mathbf{x}', \qquad (B\text{–}6)\end{aligned}$$

with operator ∇' acting on $\mathbf{x}'$ and $\chi_{\mathbb{V}}(\mathbf{x})$ being the characteristic function for $\mathbb{V}$, defined as

$$\chi_{\mathbb{V}}(\mathbf{x}) = \begin{cases} 1 & \text{for} \quad \mathbf{x}\,\text{in}\,\mathbb{V}, \\ \frac{1}{2} & \text{for} \quad \mathbf{x}\,\text{on}\,\mathbb{S}, \\ 0 & \text{for} \quad \mathbf{x}\,\text{outside}\,\mathbb{V}\cup\mathbb{S}. \end{cases} \qquad (B\text{–}7)$$

We use equation (B–6) to derive an expression for forward wave field extrapolation in the configuration of Figure B–1 (Berkhout 1985; Frazer & Sen 1985). The closed boundary $\mathbb{S}$ consists of an infinite horizontal boundary $\mathbb{S}_0$ (at $z = z_0$) and a half-sphere $\mathbb{S}_{\rm sph}$ with infinite radius ($r\to\infty$) in the upper half-space (above $\mathbb{S}_0$). The upper half-space is homogeneous; the lower half-space may be inhomogeneous. We choose the source distribution $\hat{q}(\mathbf{x}',\omega)$ in the lower half-space (below $\mathbb{S}_0$) hence outside $\mathbb{V}$. This implies that the first integral on the right-hand side of equation (B–6) vanishes. The boundary integral over the half-sphere with infinite radius also vanishes (Sommerfeld radiation condition). Hence, we are

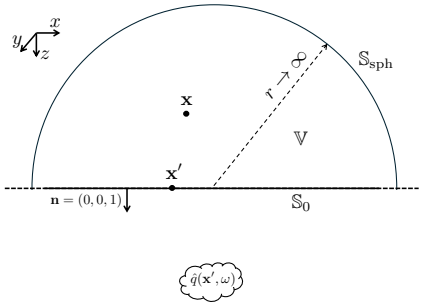

Figure B–1. *Configuration for forward wave field extrapolation (side view).*

left with a boundary integral over $\mathbb{S}_0$. At this boundary the outward pointing normal vector $\mathbf{n}$ equals $(0, 0, 1)$, hence, $\nabla' \cdot \mathbf{n} = \partial'_z$ at $\mathbb{S}_0$. Using the equation of motion $\frac{1}{\rho(\mathbf{x}')}\partial'_z \hat{p}(\mathbf{x}', \omega) = i\omega \hat{v}_z(\mathbf{x}', \omega)$, where $\hat{v}_z$ is the vertical component of the particle velocity, and the Fourier transforms of equations (A–6) and (A–14), we thus obtain

$$\chi_{\mathbb{V}}(\mathbf{x})\hat{p}(\mathbf{x}, \omega) = -\int_{\mathbb{S}_0} \Big(\hat{G}(\mathbf{x}, \mathbf{x}', \omega)\hat{v}_z(\mathbf{x}', \omega) + \hat{G}_{\rm d}(\mathbf{x}, \mathbf{x}', \omega)\hat{p}(\mathbf{x}', \omega) \Big) {\rm d}\mathbf{x}'. \qquad (B\text{–}8)$$

For $\mathbf{x}$ in the lower half-space we have $\chi_{\mathbb{V}}(\mathbf{x}) = 0$, hence, the integral on the right-hand side vanishes for this situation. For $\mathbf{x}$ in the upper half-space we have $\chi_{\mathbb{V}}(\mathbf{x}) = 1$, hence, this expression describes forward wave field extrapolation from the horizontal boundary $\mathbb{S}_0$ to any point $\mathbf{x}$ above this boundary. Since the upper half-space is homogeneous, the actual wave field ($\hat{p}$ and $\hat{v}_z$) is upward propagating at $\mathbb{S}_0$. Taking the entire medium homogeneous for the Green's function ($\hat{G}$ and $\hat{G}_{\rm d}$), then the two terms under the integral give equal contributions, hence, equation (B-8) can be replaced by

$$\hat{p}(\mathbf{x}, \omega) = -2\int_{\mathbb{S}_0} \hat{G}_{\rm d}(\mathbf{x}, \mathbf{x}', \omega)\hat{p}(\mathbf{x}', \omega) {\rm d}\mathbf{x}', \qquad (B\text{–}9)$$

for $\mathbf{x}$ in the upper half-space (Berkhout & Wapenaar 1989). Equation (B-9) is a Rayleigh integral (Rayleigh (1878) derived expressions like this to describe the radiation of sources, distributed over a plane). Transforming this back to the time domain and using the causality condition of the Green's function gives

$$p(\mathbf{x}, t) = -2\int_{\mathbb{S}_0} \int_0^\infty G_{\rm d}(\mathbf{x}, \mathbf{x}', t')p(\mathbf{x}', t - t'){\rm d}t'{\rm d}\mathbf{x}', \qquad (B\text{–}10)$$

for $\mathbf{x}$ in the upper half-space. The time integral in this expression is a convolution, which can be written in a shorter notation using the convolution symbol $*$. Equation (B-10) thus becomes

$$p(\mathbf{x}, t) = -2\int_{\mathbb{S}_0} G_{\rm d}(\mathbf{x}, \mathbf{x}', t) * p(\mathbf{x}', t){\rm d}\mathbf{x}', \qquad (B\text{–}11)$$

for $\mathbf{x}$ in the upper half-space.

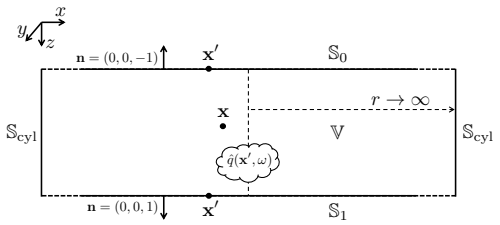

Figure C–1. *Configuration for inverse wave field extrapolation (side view).*

APPENDIX C: INVERSE WAVE FIELD EXTRAPOLATION

The Fourier transform of the time-reversed Green's function $\mathcal{G}(\mathbf{x}, \mathbf{x}', -t)$ is given by $\hat{\mathcal{G}}^*(\mathbf{x}, \mathbf{x}', \omega)$, where the superscript $*$ denotes complex conjugation. Since for a lossless medium $\hat{\mathcal{G}}^*$ obeys the same wave equation as $\hat{\mathcal{G}}$ (equation (B-3)), equation (B-6) remains valid when we replace $\hat{\mathcal{G}}$ by $\hat{\mathcal{G}}^*$ (Bojarski 1983), hence

$$\chi_{\mathbb{V}}(\mathbf{x})\hat{p}(\mathbf{x}, \omega) = -\int_{\mathbb{V}} i\omega\hat{\mathcal{G}}^*(\mathbf{x}, \mathbf{x}', \omega)\hat{q}(\mathbf{x}', \omega){\rm d}\mathbf{x}' + \oint_{\mathbb{S}} \frac{1}{\rho(\mathbf{x}')} \Big(\hat{\mathcal{G}}^*(\mathbf{x}, \mathbf{x}', \omega)\nabla'\hat{p}(\mathbf{x}', \omega) - \hat{p}(\mathbf{x}', \omega)\nabla'\hat{\mathcal{G}}^*(\mathbf{x}, \mathbf{x}', \omega) \Big) \cdot \mathbf{n}{\rm d}\mathbf{x}'. \qquad (C\text{–}1)$$

We use equation (C–1) to derive an expression for inverse wave field extrapolation in the configuration of Figure C–1. The closed boundary $\mathbb{S}$ consists of two infinite horizontal boundaries $\mathbb{S}_0$ (at $z = z_0$) and $\mathbb{S}_1$ (at $z = z_1$), connected by a cylindrical surface $\mathbb{S}_{\rm cyl}$ with infinite radius ($r \to \infty$). The half-spaces above $\mathbb{S}_0$ and below $\mathbb{S}_1$ are homogeneous; the medium between these boundaries may be inhomogeneous. We choose the source distribution $\hat{q}(\mathbf{x}', \omega)$ between the two boundaries $\mathbb{S}_0$ and $\mathbb{S}_1$, hence inside $\mathbb{V}$. The boundary integral over the cylindrical surface with infinite radius vanishes because its surface area increases with r, but its integrand decays with $1/r^2$. The outward pointing normal vector $\mathbf{n}$ equals $(0, 0, -1)$ at $\mathbb{S}_0$ and $(0, 0, 1)$ at $\mathbb{S}_1$, hence, $\nabla' \cdot \mathbf{n} = -\partial'_z$ at $\mathbb{S}_0$ and $\nabla' \cdot \mathbf{n} = \partial'_z$ at $\mathbb{S}_1$. Using again the equation of motion and the Fourier

transforms of equations (A–6) and (A–14), we thus obtain

$$\begin{aligned}\hat{p}(\mathbf{x},\omega) &= -\int_{\mathbb{V}} \hat{G}^*(\mathbf{x},\mathbf{x}',\omega)\hat{q}(\mathbf{x}',\omega)\mathrm{d}\mathbf{x}' \\ &\quad -\int_{\mathbb{S}_0}\Big(\hat{G}^*(\mathbf{x},\mathbf{x}',\omega)\hat{v}_z(\mathbf{x}',\omega) \\ &\quad -\hat{G}^*_{\mathrm{d}}(\mathbf{x},\mathbf{x}',\omega)\hat{p}(\mathbf{x}',\omega)\Big)\mathrm{d}\mathbf{x}' \\ &\quad +\int_{\mathbb{S}_1}\Big(\hat{G}^*(\mathbf{x},\mathbf{x}',\omega)\hat{v}_z(\mathbf{x}',\omega) \\ &\quad -\hat{G}^*_{\mathrm{d}}(\mathbf{x},\mathbf{x}',\omega)\hat{p}(\mathbf{x}',\omega)\Big)\mathrm{d}\mathbf{x}', \qquad (C\text{–}2)\end{aligned}$$

for $\mathbf{x}$ in $\mathbb{V}$. Since the medium above $\mathbb{S}_0$ and below $\mathbb{S}_1$ is homogeneous (for the actual wave field and for the Green's function), the two terms under each of the boundary integrals give equal contributions, hence, equation (C-2) can be replaced by

$$\begin{aligned}\hat{p}(\mathbf{x},\omega) &= -\int_{\mathbb{V}} \hat{G}^*(\mathbf{x},\mathbf{x}',\omega)\hat{q}(\mathbf{x}',\omega)\mathrm{d}\mathbf{x}' \\ &\quad +2\int_{\mathbb{S}_0} \hat{G}^*_{\mathrm{d}}(\mathbf{x},\mathbf{x}',\omega)\hat{p}(\mathbf{x}',\omega)\mathrm{d}\mathbf{x}' \\ &\quad -2\int_{\mathbb{S}_1} \hat{G}^*_{\mathrm{d}}(\mathbf{x},\mathbf{x}',\omega)\hat{p}(\mathbf{x}',\omega)\mathrm{d}\mathbf{x}', \qquad (C\text{–}3)\end{aligned}$$

for $\mathbf{x}$ in $\mathbb{V}$. Going from equation (C-2) to equation (C-3), it is assumed that evanescent waves at $\mathbb{S}_0$ and $\mathbb{S}_1$ can be ignored (Wapenaar *et al.* 1989). Transforming equation (C-3) back to the time domain and choosing a point source $q(\mathbf{x}',t) = \delta(\mathbf{x}'-\mathbf{x}_S)s(t)$ (with $\mathbf{x}_S$ in $\mathbb{V}$) gives

$$\begin{aligned}p(\mathbf{x},t) &= -G(\mathbf{x},\mathbf{x}_S,-t) * s(t) \\ &\quad +2\int_{\mathbb{S}_0} G_{\mathrm{d}}(\mathbf{x},\mathbf{x}',-t) * p(\mathbf{x}',t)\mathrm{d}\mathbf{x}' \\ &\quad -2\int_{\mathbb{S}_1} G_{\mathrm{d}}(\mathbf{x},\mathbf{x}',-t) * p(\mathbf{x}',t)\mathrm{d}\mathbf{x}', \qquad (C\text{–}4)\end{aligned}$$

for $\mathbf{x}$ in $\mathbb{V}$. Inverse extrapolation is often approximated by the second term only (Schneider 1978; Berkhout 1985), hence

$$\langle p(\mathbf{x},t)\rangle = 2\int_{\mathbb{S}_0} G_{\mathrm{d}}(\mathbf{x},\mathbf{x}',-t) * p(\mathbf{x}',t)\mathrm{d}\mathbf{x}', \qquad (C\text{–}5)$$

or, writing the integrand as a correlation integral,

$$\langle p(\mathbf{x},t)\rangle = 2\int_{\mathbb{S}_0}\int_0^\infty G_{\mathrm{d}}(\mathbf{x},\mathbf{x}',t')p(\mathbf{x}',t+t')\mathrm{d}t'\mathrm{d}\mathbf{x}', \qquad (C\text{–}6)$$

for $\mathbf{x}$ below $\mathbb{S}_0$ and above the source, see the main text for a further discussion.

APPENDIX D: EXTRAPOLATION WITH FOCUSING FUNCTIONS

Consider a configuration, consisting of an inhomogeneous lossless medium below $\mathbb{S}_0$ (at $z = z_0$), with propagation velocity $c(\mathbf{x})$ and mass density $\rho(\mathbf{x})$, and a homogeneous lossless medium above $\mathbb{S}_0$, with propagation velocity c_0 and mass density ρ_0. In the space-frequency domain, the acoustic pressure $\hat{p}(\mathbf{x},\omega)$ in this configuration obeys wave equation (B-2), with operator $\hat{\mathcal{L}}(\mathbf{x},\omega)$ defined in equation (B-4). In the following we assume that the source distribution $\hat{q}(\mathbf{x},\omega)$ is restricted to the upper half-space. Hence, for all $\mathbf{x}$ below the source distribution, $\hat{p}(\mathbf{x},\omega)$ obeys the source-free wave equation

$$\hat{\mathcal{L}}\hat{p} = 0. \qquad (D\text{–}1)$$

For the same configuration we define the Fourier-transformed focusing function $\hat{F}(\mathbf{x},\mathbf{x}',\omega)$, with $\mathbf{x}'$ denoting a focal point at $\mathbb{S}_0$ (hence, $z' = z_0$). This focusing function obeys the same source-free wave equation throughout space, hence

$$\hat{\mathcal{L}}\hat{F} = 0. \qquad (D\text{–}2)$$

Moreover, $\hat{F}(\mathbf{x},\mathbf{x}',\omega)$ is defined such that for $\mathbf{x}$ at $\mathbb{S}_0$ it obeys the Fourier transform of the focusing condition of equation (19), hence

$$\hat{F}(\mathbf{x}_{\mathrm{H}},z_0,\mathbf{x}'_{\mathrm{H}},z_0,\omega) = \delta(\mathbf{x}_{\mathrm{H}}-\mathbf{x}'_{\mathrm{H}}), \qquad (D\text{–}3)$$

with $\mathbf{x}_{\mathrm{H}}$ and $\mathbf{x}'_{\mathrm{H}}$ being the horizontal components of $\mathbf{x}$ and $\mathbf{x}'$, respectively. Finally, for $\mathbf{x}$ at and above $\mathbb{S}_0$ this focusing function propagates upward. Note that $\hat{F}^*(\mathbf{x},\mathbf{x}',\omega)$, which is the Fourier transform of the time-reversed focusing function, obeys the same wave equation and the same focusing condition as $\hat{F}(\mathbf{x},\mathbf{x}',\omega)$; for $\mathbf{x}$ at and above $\mathbb{S}_0$ it propagates downward.

For all $\mathbf{x}$ below the source distribution, we write $\hat{p}(\mathbf{x},\omega)$ as a superposition of the mutually independent focusing functions, according to

$$\begin{aligned}\hat{p}(\mathbf{x},\omega) &= \int_{\mathbb{S}_0} \hat{F}(\mathbf{x},\mathbf{x}',\omega)\hat{a}(\mathbf{x}',\omega)\mathrm{d}\mathbf{x}' \\ &\quad + \int_{\mathbb{S}_0} \hat{F}^*(\mathbf{x},\mathbf{x}',\omega)\hat{b}(\mathbf{x}',\omega)\mathrm{d}\mathbf{x}', \qquad (D\text{–}4)\end{aligned}$$

where $\hat{a}(\mathbf{x}',\omega)$ and $\hat{b}(\mathbf{x}',\omega)$ are coefficients which still need to be determined. Using the equation of motion, we obtain a similar expression for the vertical component of the

particle velocity from equation (D-4), according to

$$\begin{aligned}\hat{v}_z(\mathbf{x},\omega) &= \frac{1}{i\omega\rho(\mathbf{x})}\partial_z\hat{p}(\mathbf{x},\omega)\\ &= \frac{1}{i\omega\rho(\mathbf{x})}\int_{\mathbb{S}_0}\partial_z\hat{F}(\mathbf{x},\mathbf{x}',\omega)\hat{a}(\mathbf{x}',\omega)\mathrm{d}\mathbf{x}'\\ &+ \frac{1}{i\omega\rho(\mathbf{x})}\int_{\mathbb{S}_0}\partial_z\hat{F}^*(\mathbf{x},\mathbf{x}',\omega)\hat{b}(\mathbf{x}',\omega)\mathrm{d}\mathbf{x}'. \quad (D\text{–}5)\end{aligned}$$

We solve the coefficients $\hat{a}(\mathbf{x}',\omega)$ and $\hat{b}(\mathbf{x}',\omega)$ from the boundary conditions for $\hat{p}(\mathbf{x},\omega)$ and $\hat{v}_z(\mathbf{x},\omega)$ at $\mathbb{S}_0$. Choosing $\mathbf{x}$ at $\mathbb{S}_0$ and using equation (D-3), we obtain from equation (D-4)

$$\hat{p}(\mathbf{x}_\mathrm{H},z_0,\omega) = \hat{a}(\mathbf{x}_\mathrm{H},z_0,\omega) + \hat{b}(\mathbf{x}_\mathrm{H},z_0,\omega). \quad (D\text{–}6)$$

From equation (D-5) we obtain for $\mathbf{x}$ at $\mathbb{S}_0$

$$\begin{aligned}\hat{v}_z(\mathbf{x}_\mathrm{H},z_0,\omega) &= \frac{1}{i\omega\rho_0}\int_{\mathbb{S}_0}\partial_z\hat{F}(\mathbf{x},\mathbf{x}',\omega)|_{z=z_0}\hat{a}(\mathbf{x}',\omega)\mathrm{d}\mathbf{x}'\\ &+ \frac{1}{i\omega\rho_0}\int_{\mathbb{S}_0}\partial_z\hat{F}^*(\mathbf{x},\mathbf{x}',\omega)|_{z=z_0}\hat{b}(\mathbf{x}',\omega)\mathrm{d}\mathbf{x}'. \quad (D\text{–}7)\end{aligned}$$

We define the spatial Fourier transform of $\hat{v}_z(\mathbf{x}_\mathrm{H},z_0,\omega)$ as

$$\tilde{v}_z(\mathbf{k}_\mathrm{H},z_0,\omega) = \int_{\mathbb{S}_0}\hat{v}_z(\mathbf{x},\omega)\exp(-i\mathbf{k}_\mathrm{H}\cdot\mathbf{x}_\mathrm{H})\mathrm{d}\mathbf{x}, \quad (D\text{–}8)$$

where $\mathbf{k}_\mathrm{H} = (k_x,k_y)$ (in 3D) or $\mathbf{k}_\mathrm{H} = k_x$ (in 2D). Applying this to both sides of equation (D-7), and subsequently using $\partial_z\tilde{F}(\mathbf{k}_\mathrm{H},z,\mathbf{x}'_\mathrm{H},z_0,\omega)|_{z=z_0} = -ik_z\tilde{F}(\mathbf{k}_\mathrm{H},z_0,\mathbf{x}'_\mathrm{H},z_0,\omega)$ for the upward propagating focusing function at z_0, yields

$$\begin{aligned}\tilde{v}_z(\mathbf{k}_\mathrm{H},z_0,\omega) &= \frac{-k_z}{\omega\rho_0}\int_{\mathbb{S}_0}\tilde{F}(\mathbf{k}_\mathrm{H},z_0,\mathbf{x}',\omega)\hat{a}(\mathbf{x}',\omega)\mathrm{d}\mathbf{x}'\\ &+ \frac{k_z^*}{\omega\rho_0}\int_{\mathbb{S}_0}\tilde{F}^*(-\mathbf{k}_\mathrm{H},z_0,\mathbf{x}',\omega)\hat{b}(\mathbf{x}',\omega)\mathrm{d}\mathbf{x}', \quad (D\text{–}9)\end{aligned}$$

where the vertical wavenumber k_z is defined as

$$k_z = \begin{cases}\sqrt{\frac{\omega^2}{c_0^2}-\mathbf{k}_\mathrm{H}\cdot\mathbf{k}_\mathrm{H}}, & \text{for} \quad \mathbf{k}_\mathrm{H}\cdot\mathbf{k}_\mathrm{H}\le\frac{\omega^2}{c_0^2},\\ i\sqrt{\mathbf{k}_\mathrm{H}\cdot\mathbf{k}_\mathrm{H}-\frac{\omega^2}{c_0^2}}, & \text{for} \quad \mathbf{k}_\mathrm{H}\cdot\mathbf{k}_\mathrm{H}>\frac{\omega^2}{c_0^2}.\end{cases} \quad (D\text{–}10)$$

The two cases in the latter equation correspond to propagating and evanescent waves, respectively. Applying the spatial Fourier transform to equation (D-3) we obtain

$$\tilde{F}(\mathbf{k}_\mathrm{H},z_0,\mathbf{x}'_\mathrm{H},z_0,\omega) = \exp(-i\mathbf{k}_\mathrm{H}\cdot\mathbf{x}'_\mathrm{H}). \quad (D\text{–}11)$$

Using this in equation (D-9) gives

$$\tilde{v}_z(\mathbf{k}_\mathrm{H},z_0,\omega) = \frac{-k_z}{\omega\rho_0}\tilde{a}(\mathbf{k}_\mathrm{H},z_0,\omega) + \frac{k_z^*}{\omega\rho_0}\tilde{b}(\mathbf{k}_\mathrm{H},z_0,\omega). \quad (D\text{–}12)$$

Equation (D-12) can be combined with the spatial Fourier transform of equation (D-6) into the following matrix-vector equation

$$\begin{pmatrix}\tilde{p}(\mathbf{k}_\mathrm{H},z_0,\omega)\\ \tilde{v}_z(\mathbf{k}_\mathrm{H},z_0,\omega)\end{pmatrix} = \begin{pmatrix}1 & 1\\ \frac{k_z^*}{\omega\rho_0} & -\frac{k_z}{\omega\rho_0}\end{pmatrix}\begin{pmatrix}\tilde{b}(\mathbf{k}_\mathrm{H},z_0,\omega)\\ \tilde{a}(\mathbf{k}_\mathrm{H},z_0,\omega)\end{pmatrix}. \quad (D\text{–}13)$$

For propagating waves, i.e., for $\mathbf{k}_\mathrm{H}\cdot\mathbf{k}_\mathrm{H}\le\frac{\omega^2}{c_0^2}$, the vertical wavenumber k_z is real-valued, see equation (D-10). Hence, for propagating waves at depth z_0 we may replace k_z^* by k_z in equation (D-13). We then recognize this equation as the well-known expression for wave field composition at depth z_0 (Corones 1975; Ursin 1983; Fishman & McCoy 1984), with $\tilde{b}(\mathbf{k}_\mathrm{H},z_0,\omega) = \tilde{p}^+(\mathbf{k}_\mathrm{H},z_0,\omega)$ and $\tilde{a}(\mathbf{k}_\mathrm{H},z_0,\omega) = \tilde{p}^-(\mathbf{k}_\mathrm{H},z_0,\omega)$, where the superscripts $+$ and $-$ refer to downward and upward propagation. For evanescent waves at depth z_0, i.e., for $\mathbf{k}_\mathrm{H}\cdot\mathbf{k}_\mathrm{H}>\frac{\omega^2}{c_0^2}$, this interpretation of equation (D-13) breaks down. However, if we ignore evanescent waves at depth z_0, we obtain in the space-frequency domain $\hat{b}(\mathbf{x}'_\mathrm{H},z_0,\omega) = \hat{p}^+(\mathbf{x}'_\mathrm{H},z_0,\omega)$ and $\hat{a}(\mathbf{x}'_\mathrm{H},z_0,\omega) = \hat{p}^-(\mathbf{x}'_\mathrm{H},z_0,\omega)$. Substituting this into equation (D-4) yields

$$\begin{aligned}\hat{p}(\mathbf{x},\omega) &= \int_{\mathbb{S}_0}\hat{F}(\mathbf{x},\mathbf{x}',\omega)\hat{p}^-(\mathbf{x}',\omega)\mathrm{d}\mathbf{x}'\\ &+ \int_{\mathbb{S}_0}\hat{F}^*(\mathbf{x},\mathbf{x}',\omega)\hat{p}^+(\mathbf{x}',\omega)\mathrm{d}\mathbf{x}', \quad (D\text{–}14)\end{aligned}$$

for all $\mathbf{x}$ below the source distribution. Equation (D-14) describes extrapolation of the wave field from $\mathbb{S}_0$ to any point $\mathbf{x}$ below the source distribution. Since the source distribution is restricted to the upper half-space, equation (D-14) holds for the entire lower half-space and for a part of the upper half-space below the shallowest source. The only approximation is that evanescent waves are neglected at $\mathbb{S}_0$. Transforming this expression back to the space-time domain yields equation (23) for all $\mathbf{x}$ below the shallowest source.